

Article

Neuroinvasion and Neurotropism by SARS-CoV-2 Variants in the K18-hACE2 Mouse

Frauke Seehusen ¹, Jordan J. Clark ² , Parul Sharma ², Eleanor G. Bentley ², Adam Kirby ², Krishanthi Subramaniam ², Sabina Wunderlin-Giuliani ¹, Grant L. Hughes ³ , Edward I. Patterson ³ , Benedict D. Michael ^{4,5} , Andrew Owen ⁶ , Julian A. Hiscox ², James P. Stewart ²  and Anja Kipar ^{1,2,*} 

- ¹ Laboratory for Animal Model Pathology, Institute of Veterinary Pathology, Vetsuisse Faculty, University of Zurich, 8057 Zurich, Switzerland; frauke.seehusen@uzh.ch (F.S.); sabina.wunderlin@vetpath.uzh.ch (S.W.-G.)
- ² Department of Infection Biology and Microbiomes, Institute of Infection, Veterinary and Ecological Sciences, University of Liverpool, Liverpool L3 5RF, UK; jordan.clark@liverpool.ac.uk (J.J.C.); parul.sharma@liverpool.ac.uk (P.S.); e.bentley@liverpool.ac.uk (E.G.B.); adam.kirby@liverpool.ac.uk (A.K.); k.subramaniam@liverpool.ac.uk (K.S.); julian.hiscox@liverpool.ac.uk (J.A.H.); j.p.stewart@liverpool.ac.uk (J.P.S.)
- ³ Departments of Vector Biology and Tropical Disease Biology, Centre for Neglected Tropical Disease, Liverpool School of Tropical Medicine, Liverpool L3 5QA, UK; grant.hughes@lstmed.ac.uk (G.L.H.); ian.patterson@lstmed.ac.uk (E.I.P.)
- ⁴ Department of Clinical Infection Microbiology and Immunology and NIHR Health Protection Research Unit in Emerging and Zoonotic Infections, Institute of Infection, Veterinary, and Ecological Sciences, University of Liverpool, Liverpool L69 7BE, UK; benedict.michael@liverpool.ac.uk
- ⁵ Department of Neurology, The Walton Centre NHS Foundation Trust, Liverpool L9 7AL, UK
- ⁶ Department of Pharmacology and Therapeutics, Centre of Excellence in Long-Acting Therapeutics (CELT), University of Liverpool, Liverpool L3 3NY, UK; aowen@liverpool.ac.uk
- * Correspondence: anja.kipar@uzh.ch



Citation: Seehusen, F.; Clark, J.J.; Sharma, P.; Bentley, E.G.; Kirby, A.; Subramaniam, K.; Wunderlin-Giuliani, S.; Hughes, G.L.; Patterson, E.I.; Michael, B.D.; et al. Neuroinvasion and Neurotropism by SARS-CoV-2 Variants in the K18-hACE2 Mouse. *Viruses* **2022**, *14*, 1020. <https://doi.org/10.3390/v14051020>

Academic Editor: F. Javier Salguero

Received: 31 March 2022

Accepted: 9 May 2022

Published: 11 May 2022

Publisher's Note: MDPI stays neutral with regard to jurisdictional claims in published maps and institutional affiliations.



Copyright: © 2022 by the authors. Licensee MDPI, Basel, Switzerland. This article is an open access article distributed under the terms and conditions of the Creative Commons Attribution (CC BY) license (<https://creativecommons.org/licenses/by/4.0/>).

Abstract: Severe Acute Respiratory Syndrome Coronavirus 2 (SARS-CoV-2) not only affects the respiratory tract but also causes neurological symptoms such as loss of smell and taste, headache, fatigue or severe cerebrovascular complications. Using transgenic mice expressing human angiotensin-converting enzyme 2 (hACE2), we investigated the spatiotemporal distribution and pathomorphological features in the CNS following intranasal infection with SARS-CoV-2 variants, as well as after prior influenza A virus infection. Apart from Omicron, we found all variants to frequently spread to and within the CNS. Infection was restricted to neurons and appeared to spread from the olfactory bulb mainly in basally oriented regions in the brain and into the spinal cord, independent of ACE2 expression and without evidence of neuronal cell death, axonal damage or demyelination. However, microglial activation, microgliosis and a mild macrophage and T cell dominated inflammatory response was consistently observed, accompanied by apoptotic death of endothelial, microglial and immune cells, without their apparent infection. Microgliosis and immune cell apoptosis indicate a potential role of microglia for pathogenesis and viral effect in COVID-19 and the possible impairment of neurological functions, especially in long COVID. These data may also be informative for the selection of therapeutic candidates and broadly support the investigation of agents with adequate penetration into relevant regions of the CNS.

Keywords: Severe Acute Respiratory Syndrome Coronavirus 2; mouse model; COVID-19; encephalitis; microgliosis; influenza A virus coinfection; virus variants

1. Introduction

As of March, 2022, the newly emerged betacoronavirus, Severe Acute Respiratory Syndrome Coronavirus-2 (SARS-CoV-2), has infected over 476 million people globally, with over 6.1 million deaths due to the associated disease, COVID-19 (WHO, COVID-19 Dashboard, 27 March 2022). The majority of COVID-19 patients display respiratory symptoms;

however, a proportion of patients mostly develop transient unspecific neurological signs such as loss of smell and taste (anosmia, ageusia), headache or dizziness. Fatal cases can also be associated with ischemic stroke, hemorrhagic encephalopathy and epileptic seizures as well as meningoencephalitis [1–7].

There is evidence of viral entry into the brain through the olfactory or vagal nerve and/or the oral and ophthalmic routes, with trans-synaptic neuronal spread to other brain regions [8–10]; this could provide a link to the frequently reported (initial) anosmia and ageusia. However, sparing of the olfactory bulb despite infection of olfactory and nasal mucosa was also detected [11]. In addition, hematogenous spread to the brain via infection of endothelial cells and/or immune cells has been suspected, though this has since been disputed [12–14].

Pathomorphological findings reported in the brain of fatal human COVID-19 cases are variable and present as vascular/hemodynamic/ischemic lesions such as ischemic infarcts and/or mild inflammatory changes; neuronal or axonal damage and acute disseminated encephalomyelitis have been reported in rare cases [9,15–22]. Focal or diffuse microglial activation or microglial nodules have also been observed [9,15–17,20,23,24]. COVID-19 patients can harbor SARS-CoV-2 RNA and protein in the brain [9,10,25], and a study using human brain organoids provided strong evidence that SARS-CoV-2 replicates in neurons [26]. However, the presence of the virus was not found to be associated with the severity of neuropathological changes [9], and a report on 18 patients failed to detect SARS-CoV-2 antigen by immunohistochemical staining although low levels of viral RNA were detected by RT-PCR in five patients [21]. Another study found viral RNA in the leptomeningeal layer surrounding the olfactory bulb and interpreted this finding as evidence against the potential neurotropic properties and neuroinvasive capacity of SARS-CoV-2 [11].

Encephalopathy, as a severe complication in COVID-19, is often associated with systemic hyperinflammation mainly provoked by an aberrantly excessive innate immune response [27]. It is suspected that not only a direct virus-induced endotheliitis, but also a maladaptive innate immune response may impair neurovascular endothelial function and cause disruption of the blood–brain barrier (BBB), activation of innate immune signalling pathways and a parainfectious autoimmunity [27]. However, infection of endothelial cells has subsequently been questioned [14], thereby it is still awaiting final proof or refute.

The role of glial cells in COVID-19 encephalopathies has also been discussed [28,29]. Glial cells might not only represent potential targets for viral infection but are also highly sensitive to systemic proinflammatory cytokines [30–32]. In COVID-19 patients, the massive systemic release of inflammatory cytokines could affect endothelial cells and astrocytes of the BBB, thus, facilitating viral entry similar to other viral brain diseases, such as HIV-1 encephalitis and measles [33]. Indeed, it has been shown that SARS-CoV-2 spike protein S1 from the blood can pass the BBB and thereby gain access to the brain parenchyma in mice, potentially triggering a parenchymal response without the presence of the intact virus [34]. Furthermore, astrocytes and microglia may contribute to the local neuroinflammatory response of the CNS [28,35]. SARS-CoV-2 infection of astrocytes has been described in human brains [36]. Additionally, microglial cells are hypothesized to be involved in the innate immune response and facilitate viral clearance, the recruitment of immune cells as well as the activation of antiviral responses and cytokine production in the brain of COVID-19 patients [29]. Some authors also propose that a SARS-CoV-2-induced proinflammatory microglial phenotype might contribute to the development of subsequent neurodegenerative disorders [37,38]. Furthermore, the proinflammatory priming of microglia, either by direct SARS-CoV-2 infection or a peripheral cytokine storm, could exacerbate disease, as indicated in experimental murine coronavirus (MHV-A59) infection [39].

The human angiotensin-converting enzyme 2 (hACE2) is considered to be the main host receptor for SARS-CoV-2, binding to the viral spike protein (S) [40]. The K18-hACE2 transgenic (K18-hACE2) mouse, where hACE2 expression is driven by the epithelial cell cytokeratin-18 (K18) promoter, developed to study the pathogenesis of SARS-CoV in-

fection [41], is frequently employed to address a broad range of questions regarding SARS-CoV-2, as the expression of hACE2 appears to convey higher binding affinity than its murine counterpart. Several studies have shown that intranasal SARS-CoV-2 infection of K18-hACE2 mice reaches the brain where it spreads widely. Infection of the brain can be associated with non-suppurative (meningo)encephalitis [26,42–44]. With high infectious doses (10^5 PFU), very high viral loads were found in the brain at a time when lung burdens had already decreased, in association with the upregulation of IFN- α as well as proinflammatory cytokine and chemokine transcription; the authors proposed that clinical symptoms or lethal outcome of infection in these mice was a consequence of neuroinvasion [44,45]. Another study using an even higher viral inoculum (10^6 PFU) elicited CNS signs (tremors, proprioceptive defects, abnormal gait, imbalance) by day 6/7 after infection [42]. Studies in mice have also confirmed that the virus access the brain via the olfactory bulb [26,34].

Detailed information on the effect of SARS-CoV-2 in the brain of COVID-19 patients has so far been collected from fatal cases. However, there is a current paucity of data relating to what happens in the brain of patients that do not have severe disease, recover from it or develop long COVID. A better understanding of the viral dynamics within the CNS will provide further insight into the disease pathogenesis and will be highly informative for therapeutics development by providing insight into the prerequisites for distribution of new medicines in development. The present study represents an attempt to address this question by investigating the CNS of K18-hACE2 mice after intranasal infection with low to moderate doses of SARS-CoV-2 strains, and also in combination with prior influenza A virus infection as it might foster neuronal spread [43].

2. Materials and Methods

2.1. Cell Culture and Viruses

A Pango lineage B strain of SARS-CoV-2 (hCoV-2/human/Liverpool/REMRQ0001/2020) cultured from a nasopharyngeal swab from a patient, was passaged in Vero E6 cells [46]. The fourth virus passage (P4) was used for infections after it had been checked for deletions in the mapped reads and the stock confirmed to not contain any deletions that can occur on passage [43].

Human nCoV19 isolate/England/202012/01B (lineage B.1.1.7; Alpha variant) was from the National Infection Service of Public Health England, Porton Down, UK via the European Virus Archive (catalogue code 004V-04032). This was supported by the European Virus Archive GLOBAL (EVA-GLOBAL) project that has received funding from the European Union's Horizon 2020 research and innovation programme under grant agreement No 871029.

B.1.351 (Beta variant: 20I/501.V2.HV001) isolate [47] was received at P3 from the Centre for the AIDS Programme of Research in South Africa (CAPRISA), Durban, in Oxford in January, 2021, passaged in VeroE6/TMPRSS2 cells (NIBSC reference 100978), used here at P4. Identity was confirmed by deep sequencing at the Wellcome Trust Centre for Human Genetics, University of Oxford.

The B.1.617.2 (Delta variant) hCoV-19/England/SHEF-10E8F3B/2021 (GISAID accession number EPI_ISL_1731019) was kindly provided by Prof. Wendy Barclay, Imperial College London, London, UK, through the Genotype-to-Phenotype National Virology Consortium (G2P-UK). Sequencing confirmed it contained the spike protein mutations T19R, K77R, G142D, Δ 156-157/R158G, A222V, L452R, T478K, D614G, P681R, D950N. The B.1.1.529/BA.1 (Omicron variant) isolate M21021166 was originally isolated by Prof. Gavin Screaton, University of Oxford, UK [48], and then obtained from Prof. Wendy Barclay, Imperial College London, London, UK, through G2P-UK. Sequencing confirmed it contained the spike protein mutations A67V, Δ 69-70, T95I, G142D/ Δ 143-145, Δ 211/L212I, ins214EPE, G339D, S371L, S373P, S375F, K417N, N440K, G446S, S477N, T478K, E484A, Q493R, G496S, Q498R, N501Y, Y505H, T547K, D614G, H655Y, N679K, P681H, N764K, A701V, D796Y, N856K, Q954H, N969K, L981F.

Details of the sequencing protocols have been reported previously [43].

The titers of all isolates were confirmed on Vero E6 cells, and the sequences of all stocks confirmed.

Influenza virus A/HKx31 (X31, H3N2) was propagated in the allantoic cavity of 9-day-old embryonated chicken eggs at 35 °C. Titers were determined by an influenza plaque assay using MDCK cells [43].

2.2. Biosafety

All work was performed in accordance with risk assessments and standard operating procedures approved by the University of Liverpool Biohazards Sub-Committee and by the UK Health and Safety Executive. Work with SARS-CoV-2 was performed at containment level 3 by personnel equipped with respirator airstream units with filtered air supply.

2.3. Animals and Virus Infections

Animal work was approved by the local University of Liverpool Animal Welfare and Ethical Review Body and performed under UK Home Office Project Licence PP4715265. Mice carrying the human ACE2 gene under the control of the keratin 18 promoter (K18-hACE2; formally B6.Cg-Tg (K18-ACE2) 2PrImn/J) were purchased from Jackson Laboratories and Charles River. Mice were maintained under SPF barrier conditions in individually ventilated cages.

For each experiment, animals were randomly assigned into multiple groups. For SARS-CoV-2 infection, mice were anaesthetized lightly with isoflurane and inoculated intra-nasally with 50 µL containing 10³ PFU or 10⁴ PFU (cohort 3; Pango lineage B) SARS-CoV-2 in PBS (Table 1); control animals received PBS. For double infections (cohort 2), mice were anaesthetized lightly with KETASET i.m. and inoculated intranasally with 10² PFU IAV X31 in 50 µL sterile PBS. Three days later, they were infected with SARS-CoV-2 (Pango lineage B), as described above. Mock-infected mice served as controls.

Table 1. Study cohorts. All viruses, unless otherwise stated, are SARS-CoV-2 strains. Animal numbers differ, as for some cohorts, mice originated from several experiments. For SARS-CoV-2 Alpha and Beta, only a few animals were examined to determine whether the strain can also spread to the brain. In Cohort 3, SARS-CoV-2 Pango lineage B infection took place 3 days after IAV infection.

Cohort	Virus 1		Virus 2		DPI (pos)
	Virus	PFU	Virus	PFU	
1	Pango B	10 ⁴	-	-	3 (0/4), 7 (7/9)
2	IAV X31	10 ²	Pango B	10 ⁴	3 (0/4), 7 (3/4)
3	Pango B	10 ³	-	-	6 (6/6)
4	Alpha	10 ³	-	-	3 (0/4), 6 (2/2)
5	Beta	10 ³	-	-	3 (2/4), 6 (2/2)
6	Delta	10 ³	-	-	3 (0/4), 5 (6/8), 6 (3/6), 7 (5/6)
7	Omicron BA.1	10 ³	-	-	5 (0/5), 6 (0/6), 7 (0/6)

Abbreviations: DPI—day post-infection; PFU—plaque forming units; pos—no of animals with viral infection of the brain confirmed by immunohistochemistry for viral nucleoprotein of those infected intranasally with the virus.

Mice were monitored for any clinical signs and weighed. Animals were sacrificed at 3, 5, 6 or 7 days post-SARS-CoV-2 infection (Table 1) by an overdose of pentobarbitone. Mice were dissected and tissues collected immediately for downstream processing; the lungs were processed for other studies [43,49,50].

2.4. Tissue Collection, Preparation and Processing

The heads from all animals and the spinal cords (C1-T12) of selected animals of cohorts 1 and 2 were collected and fixed in 10% neutral buffered formal saline for between 24 and 48 h. For cohorts 1, 2, 4, 5 and part of cohort 6, brains were exenterated, and

coronal sections prepared. Heads were then sawn longitudinally in the midline using a diamond saw (Exakt 300; Exakt Advanced Technologies GmbH, Norderstedt, Germany) for histological assessment of the nasal cavity, cribriform plate and rostral parts of the olfactory bulb that had not been removed with the brain. For all other animals, heads were sawn longitudinally in the midline and the brain left in the skull. In cases from cohorts 1 and 2, where SARS-CoV-2 viral antigen was detected in the brain (see below), the spinal cords were sawn into approximately 1.5 mm thick cross sections. Heads and spinal cord sections were gently decalcified in RDF (Biosystems Switzerland AG, Muttenz, Switzerland) for 5 days, at room temperature (RT) and on a shaker, twice. Brains, heads and spinal cords were routinely embedded in paraffin wax.

2.5. Histology, Immunohistology

Consecutive sections (3–5 µm) were either stained with hematoxylin and eosin (HE) or used for immunohistochemistry (IH). IH was performed using the horseradish peroxidase (HRP) method to detect the viral antigen in all examined tissues in all animals, and in selected cases to identify macrophages/activated microglial cells (Iba1+), T cells (CD3+), B cells (CD45R/B220+) and neutrophils (Ly6G+) and to highlight astrocytes (glial fibrillary acidic protein, GFAP+), apoptotic cells (cleaved caspase 3+), disturbances of the fast axonal transport indicating acutely damaged neuronal axons (amyloid precursor protein, APP+) and ACE2 expression in selected animals where the viral antigen was detected in the brains. Antibodies and detection systems are listed in Supplemental Table S1. Briefly, after deparaffination, sections underwent antigen retrieval in citrate buffer (pH 6.0) or Tris/EDTA buffer (pH 9) for 20 min at 98 °C, followed by incubation with the primary antibodies (diluted in dilution buffer, Agilent Dako). This was followed by the blocking of endogenous peroxidase (peroxidase block, Agilent Dako) for 10 min at RT and incubation with the appropriate secondary antibodies/detection systems, all in an autostainer (Dako Agilent or Ventana). Sections were subsequently counterstained with hematoxylin.

The brain of a mock-infected control hACE mouse served as the normal brain control for ACE2, GFAP and APP, and a lymph node from a normal mouse for the leukocyte and apoptosis markers. Sections from the lungs served as internal positive controls for SARS-CoV-2 and IAV antigen expression, and sections incubated without the primary antibodies served as negative controls.

2.6. RNA In Situ Hybridization (RNA-ISH)

In selected cases, RNA ISH was performed using the RNAscope[®] ISH method (Advanced Cell Diagnostics (ACD Advanced Cell Diagnostics, Newark, CA, USA)) and the RNAscope[®] 2.5 Detection Reagent Kit (Brown) according to the manufacturer's protocol and as previously described [51,52]. All cases were first tested for the suitability of the tissue (RNA preservation and quality) with an oligoprobe for *Mus musculus* peptidylprolyl isomerase B (PPIB) mRNA (ACD). Those yielding good PPIB signals were then subjected to RNA-ISH for nCoV2019-S (coding for Wuhan seafood market pneumonia virus isolate Wuhan-Hu-1 complete genome; Genbank NC_045512.2). Briefly, sections were heated to 60 °C for 1 h and subsequently deparaffinized. Permeabilization was achieved by incubating the section in pretreatment solution 1 (RNAscope[®] Hydrogen Peroxide) for 10 min at RT, followed by boiling in RNAscope[®] 1X Target Retrieval Reagents solution at 100 °C for 15 min and washing in distilled water and ethanol. After digestion with RNAscope[®] Protease Plus for 30 min at 40 °C, sections were hybridized with the oligoprobes at 40 °C in a humidity control tray for 2 h (HybEZTM Oven, ACD). Thereafter, a serial amplification with different amplifying solutions (AMP1, AMP2, AMP3, AMP4: alternating 15 min and 30 min at 40 °C) was performed. Between each incubation step, slides were washed with washing buffer. They were subsequently incubated with AMP 5, AMP 6 and DAB at RT for 30 and 15 min, respectively. Gill's hematoxylin served to counterstain the sections, which were then dehydrated with graded alcohol and xylene and coverslipped. A lung section

from an infected mouse at 3 dpi served as a positive control. The negative control was consecutive sections incubated accordingly but without including the hybridization step.

3. Results

3.1. *In K18-hACE2 Mice, SARS-CoV-2 Pango B, Alpha, Beta and Delta Variant Infection Is Frequently Accompanied by Virus Spread into the Central Nervous System*

To assess whether SARS-CoV-2 gains access to the CNS after intranasal infection with a low to medium viral dose we examined groups of K18-hACE2 mice that had been infected with SARS-CoV-2 Pango lineage B (a variant from the initial outbreak in the UK, strain hCoV-19/England/Liverpool_REMRQ0001/2020 [43], at 10^3 and 10^4 PFU; an Alpha variant (B.1.1.7), a Beta variant (B.1.351), a Delta variant (B1.617.2) and a near clinical (B.1.1.529) Omicron variant isolate from the UK [48] (all at 10^3 PFU). In addition, we examined mice that had been infected with Pango lineage B inoculum (10^4 PFU) at day 3 post-intranasal infection with 10^2 PFU IAV (strain A/X31). SARS-CoV-2 infected mice began to lose weight at 3 or 4 dpi and continued to lose weight until the end of the experiment at 5, 6 or 7 dpi, with the exception of the Omicron infected animals which recovered from the weight loss by day 6 (Supplemental Figure S1) [43,49,50]. In the sequential IAV and Pango lineage B infected mice as well as some delta variant infected mice, the weight loss was accelerated leading to more rapid and higher mortality, as determined by a humane endpoint of 20% weight loss [43].

At day 3 post-intranasal Pango lineage B, Alpha, Beta and Delta variant infection, the viral antigen was detected in numerous individual and aggregates of occasionally degenerate epithelial cells in the nasal cavity in all SARS-CoV-2 infected animals and in two of the four IAV and Pango lineage B double infected animals. The viral antigen was also found in the lungs, in both type I and II pneumocytes in randomly distributed and variably sized patches of alveoli, with only occasional degenerate cells. This was associated with a mild increase in interstitial cellularity, endothelial cell activation with rolling, emigration and perivascular aggregation of some lymphocytes, and small macrophage aggregates, all as previously reported by this group [43]. In dual infections, identical SARS-CoV-2-associated lesions were present within areas unaffected by IAV lesions. At this stage, the SARS-CoV-2 antigen was occasionally detected in the olfactory epithelium. It was generally not observed in brain nerves and the brain, including the olfactory bulb; however, the two Beta variant infected mice exhibited several positive neurons in the olfactory bulb and patches of positive neurons in the frontal cortex and brain stem, respectively (Figure 1). In dual infected animals, IAV antigen expression was not detected in these structures either and there were no histological changes.

At days 5, 6 and 7 post-infection, the respiratory and olfactory epithelium of the nasal mucosa still exhibited viral antigen expression, more extensive in the Pango lineage B, Alpha, Beta and Delta variant than in Omicron infected mice, as confirmed by differences in viral loads detected in throat swabs [49], and decreasing with time. Infected cells generally appeared unaltered. At day 5 (studied in Delta and Omicron infected mice), the lungs of the Delta variant infected mice exhibited a mild to moderate multifocal to diffuse increase in interstitial cellularity, mild to moderate mononuclear vasculitis with lymphocyte-dominated perivascular infiltrates and multiple larger focal areas with occasional degenerate epithelial cells and some infiltrating lymphocytes, with viral antigen expression in both type I and II pneumocytes (Supplemental Figure S2). Omicron infected mice exhibited only mild pulmonary changes, with a mild patchy increase in interstitial cellularity, mild perivascular lymphocyte infiltrate and several disseminated patches of unaltered appearing alveoli with antigen-positive pneumocytes. At both 6 dpi (studied in infections with all variants) and, less severely, 7 dpi (studied in Pango lineage B, Delta and Omicron infected mice), the lungs of the Pango lineage B, Alpha, Beta and Delta variant infected animals exhibited changes similar to those described for day 5 post-infection (Supplemental Figure S2); these have been reported previously in more detail [43,49,50]. Viral antigen expression was restricted to type I and II pneumocytes of unaltered appearing alveoli and in some

infiltrating macrophages. In Omicron infected animals, the lung parenchyma was widely unaltered, though there were focal changes similar to those seen with the other strains; viral antigen expression was observed in the same cell types, though in few and smaller patches of alveoli, as recently reported [49].

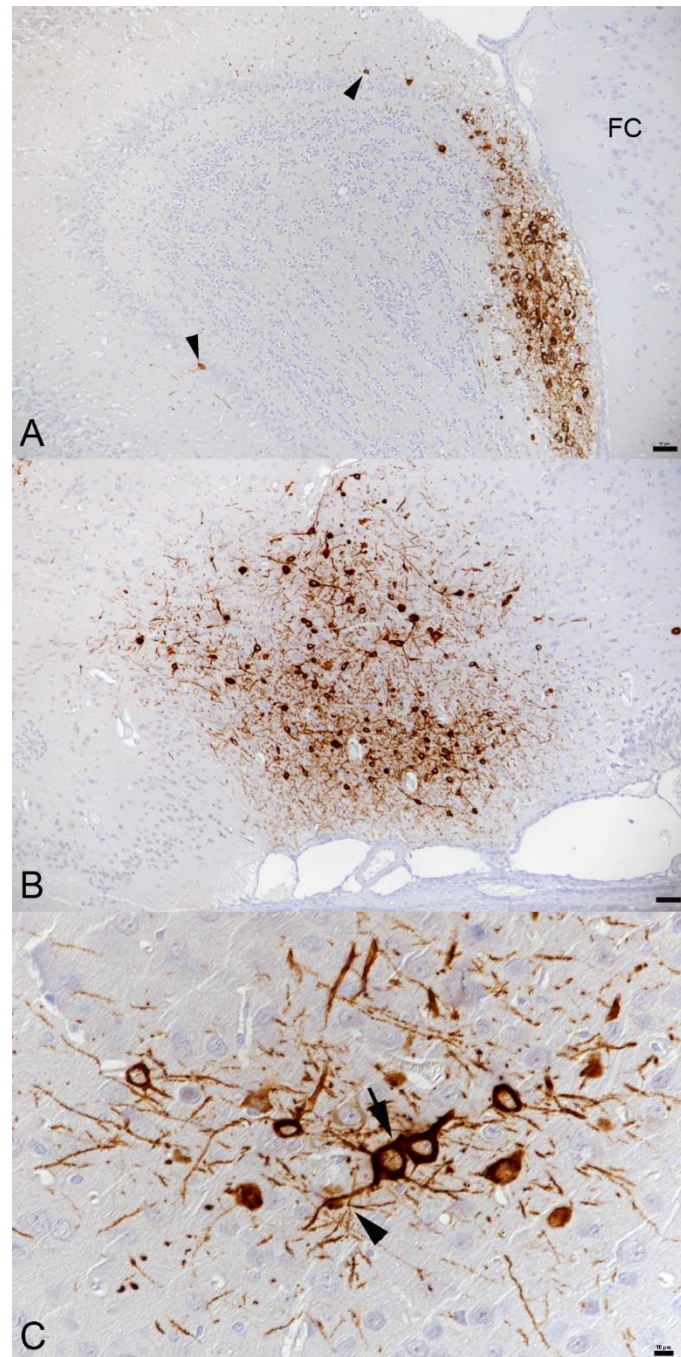


Figure 1. Brain, K18-hACE mice, day 3 post-intranasal infection with SARS-CoV-2 Beta variant at 10^3 PFU. (A) Olfactory bulb. Viral antigen is detected in a large patch of neurons in granule layer, inner and outer plexiform layer, mitral layer and glomerular layer and scattered individual neurons. FC—frontal cortex. Bar = 50 μ m. (B) Brain stem (anterior olfactory nucleus). Large patch of positive neurons. Bar = 50 μ m. (C) Cortex, same animal as in B. Patch of positive neurons with viral antigen expression in both cell body and processes. Neurons (arrow) and neuronal processes (arrowhead) often appear close apposed. Bar = 10 μ m. Immunohistochemistry, hematoxylin counterstain.

At day 5 (studied in Delta and Omicron infected animals), infection of the brain was seen in most Delta variant infected animals, i.e., both mice that had to be sacrificed at this day as they had reached the humane endpoint (20% weight loss), and four of the five scheduled sacrificed animals. In all positive animals, viral antigen expression was found in numerous patches of neurons in all basal regions, stretching from there towards the cortex. In the Omicron infected mice examined at this time point, there was no evidence of brain infection. Viral antigen expression in the brain was often seen together with its expression in the main olfactory epithelium and the olfactory bulb (Figure 2A).

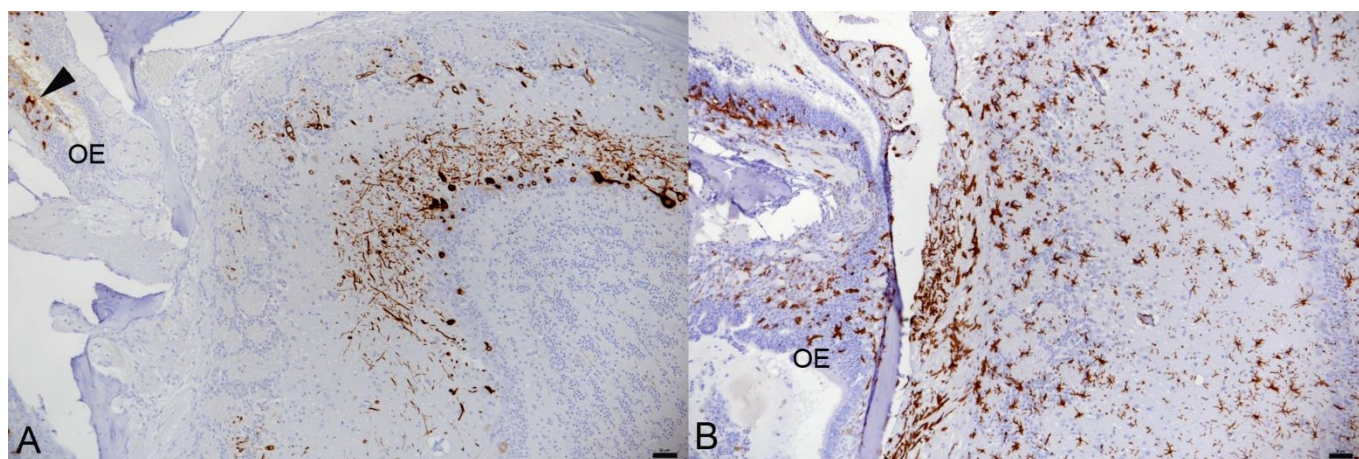


Figure 2. Olfactory bulb, K18-hACE2 mice, day 5 post-intranasal infection with SARS-CoV-2 Delta variant at 10^3 PFU. Animal with infection of the brain. Consecutive sections showing extensive viral antigen expression in neurons in glomerular, mitral cell and granular cell layer (A) and microglial activation as indicated by the morphology and strong Iba1 expression of microglial cells which is strongest in the olfactory nerve layer (arrow) (B). The olfactory epithelium (OE) exhibits several infected epithelial cells (A, arrowhead) and mild macrophage (Iba1+) infiltration (B).

At day 6, 3 of the 6, Delta variant infected mice exhibited infection of the brain, whereas all 6 Pango lineage B and both Alpha and Beta variant infected mice were found to be positive. At 7 dpi, in Pango lineage B infected animals, the viral antigen was detected in the brain of seven of the nine mice and three of the four IAV co-infected mice (all had received 10^4 PFU). The IAV antigen was not detected in the brain of double infected animals. Of the six Delta variant infected mice examined at this time point, five were positive in the brain. Again, infection of the brain was often seen together with viral antigen expression in the main olfactory epithelium and the olfactory bulb (Figure 3A).

In none of the Omicron infected animals was there any evidence of viral antigen expression in brain nerves and brain, including the olfactory bulb at 5, 6 or 7 dpi.

3.2. In K18-hACE2 Mice, SARS-CoV-2 Infection in the Central Nervous System Is Restricted to Neurons and Spreads in the Brain and into the Spinal Cord

In the present study, all animals that were examined from day 5 post-infection onwards found to harbor the viral antigen in the brain showed widespread neuronal expression but with a variable extent and with some evidence of a time dependent manner.

The two Delta variant infected mice that had to be sacrificed at day 5 post-infection due to humane endpoint (20% weight loss) exhibited patches of positive neurons in the olfactory bulb (Figure 2) as well as all basal regions and stretching from there to the cortex, sparing the cerebellar cortex.

All Pango lineage B, Alpha and Delta variant infected mice found to harbor the virus in the brain at 6 dpi exhibited positive neurons in the olfactory bulb, cortex, brain stem, hippocampus and medulla. In the Delta variant infected animals, a marked increase in the number of positive neurons was observed in comparison to 5 dpi. Mice infected with the

Beta variant showed a higher variability in the number of positive neurons, with patches of positive neurons in the basal regions and cerebral cortex sparing the cerebellum.

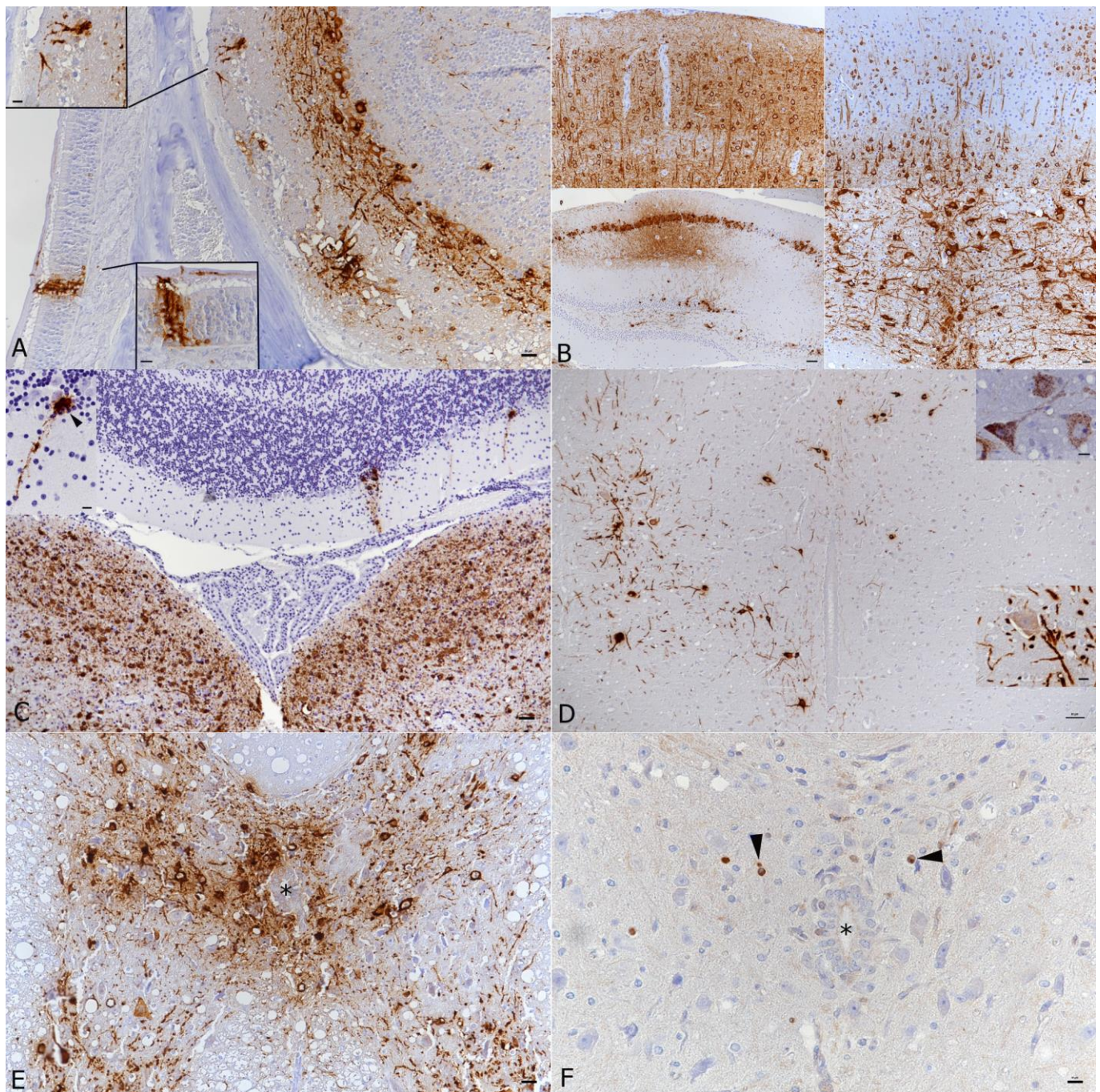


Figure 3. Brain and spinal cord, K18-hACE mice, day 7 post-intranasal SARS-CoV-2 Pango lineage B infection (10^4 PFU as single infection, or as double infection after initial infection with IAV (10^2 PFU IAV strain A/X31)). (A) Double infected animal, main olfactory epithelium (MOI), cribriform plate and olfactory bulb. Viral antigen is detected in olfactory neurons and basal cells of the MOI and in granule layer, inner and outer plexiform layer, mitral layer as well as glomerular layer of the olfactory bulb. Bar = 20 μ m. (B) Double infected animal, examples of viral antigen expression in different brain regions. Top: frontal cortex with viral antigen expression in almost all neurons (left) and mid cortex with proportion of positive neurons (right); bar = 20 μ m. Bottom: patchy virus antigen expression in the hippocampus (CA1 and CA3; left; bar = 50 μ m) and strong expression in the medulla oblongata

(right; bar = 20 μm). (C) Single infected animal, medulla oblongata and cerebellum. Viral RNA is abundantly expressed in neurons in the medulla oblongata (vestibular nuclei). The cerebellar cortex exhibits a few positive Purkinje cells (see also inset). Bar = 50 μm . (D) Single infected animal, thoracic spinal cord. The gray matter exhibits numerous neurons that express viral antigen (large image and bottom inset) and viral RNA (top inset) in cell body and processes. Bar = 50 μm . (E,F) Double infected animal, thoracic spinal cord. There is extensive viral antigen expression in neurons in the gray matter (E). Consecutive section showing scattered apoptotic (cleaved caspase 3 positive) glial cells (F, arrowheads), among intact neurons and in the absence of an inflammatory reaction. *—Central canal. Bars = 20 μm . Immunohistochemistry and RNA-ISH, hematoxylin counterstain.

At 7 dpi, in Delta variant infected mice, the number of positive neurons was slightly lower than at 6 dpi, and their distribution was patchier. In Pango lineage B infected mice, of which a total of 13 infected brains at 7 dpi were included, a strong, nearly diffuse (in affected regions) bilateral immunoreactivity of neurons was detected. In these animals, the extent of infection in the olfactory bulb was investigated more closely. Expression was variable and ranged from individual to numerous positive neurons (individual cells/neuronal processes in the olfactory nerve layer, glomerular layer, almost all cells in the external plexiform layer, individual cells in the mitral cell layer), and sometimes also aggregates of positive sensory neuronal cells and their dendrites in the olfactory epithelium layer of the main olfactory epithelium (MOE; Figure 3A). None of the animals exhibited a reaction in cranial nerves or the inner ear.

Overall, the viral antigen was detected in a widespread manner across most brain regions in all infected animals with all virus variants apart from Omicron (Figure 3B, Supplemental Figure S2). Positive neurons were found among others in the anterior olfactory nucleus, primary and secondary motor area, primary somatosensory area, anterior cingulate area, gustatory area, auditory area, infralimbic area, lateral and medial septal nucleus, caudoputamen, piriform area, visual area, ectorhinal area, entorhinal area, retrosplenial area, hippocampus and dentate gyrus, subiculum, nearly all midbrain nuclei, thalamus/hypothalamus, amygdalar nuclei, nucleus accumbens, several cranial nerve nuclei (trigeminal, vestibular, hypoglossal nuclei), reticular nucleus, cuneate nucleus, dentate nucleus. These areas are depicted in a 3D reference atlas of the Allen Mouse Brain Common Coordinate Framework [53] (open access). The viral antigen expression was most intense in the midbrain. The cerebellum showed only individual or small groups of SARS-CoV-2 positive neurons in a few individual animals (Figure 3C).

Pango lineage B and IAV double infected animals displayed a similar infection of neurons in nearly all brain regions; the expression appeared more widespread overall than in single infected animals.

We also examined the cervical and thoracic spinal cord in the Pango lineage B single and IAV double infected animals. Indeed, the virus had spread to the spinal cord where it was found in neurons in the gray matter (motor neurons and sensory neurons; Figure 3D,E), stretching through the entire cervical and thoracic spinal cord, or decreasing progressively from the cervical spinal cord.

RNA-ISH yielded similar results as immunohistology (Figure 3C), confirming widespread neuronal infection accentuated in the midbrain.

3.3. SARS-CoV-2 Infection of the Brain Is Associated with Diffuse Microglial Activation and a Mild Macrophage and T Cell Dominated Inflammatory Response

In animals where the virus was detected in neurons in the brain at 3 and 5 dpi of Pango lineage B and at 5 dpi of the Delta variant infection, this was not associated with any histopathological changes. However, infection in the olfactory bulb was found to be associated with diffuse microglial activation in the area (Figure 2B). At 6 and 7 days post-Pango lineage B infection, a mild nonsuppurative (meningo)encephalitis was consistently observed. The inflammation was only present in areas with SARS-CoV-2 infected neurons. Therefore, it was most pronounced in frontal coronary sections of caudoputa-

men and the thalamus/hypothalamus region as well as in the hippocampal area where it was represented by the infiltration of the wall and the perivascular space of small veins by predominantly mononuclear cells, accompanied by a mild increase in parenchymal cellularity (Figure 4A). The majority of cells in the (peri)vascular infiltrates were Iba1-positive macrophages (Figure 4B). These were accompanied by T cells (CD3+) which comprised up to approximately 30% of the perivascular cells (Figure 4C). Individual T cells were also found in the neuroparenchyma, mostly in proximity to perivascular infiltrates (Figure 4C). The vascular infiltrates contained rare individual neutrophils (Ly6G+) and B cells (CD45R/B220+); Figure 4D). Animals infected with Alpha (6 dpi), Beta (6 dpi) and Delta (6 and 7 dpi) variants, and also the Pango lineage B and IAV double infected animals, exhibited a similar inflammatory reaction, both in extent and composition. Omicron infected with (all negative for viral antigen) did not exhibit any histological changes in the brain.

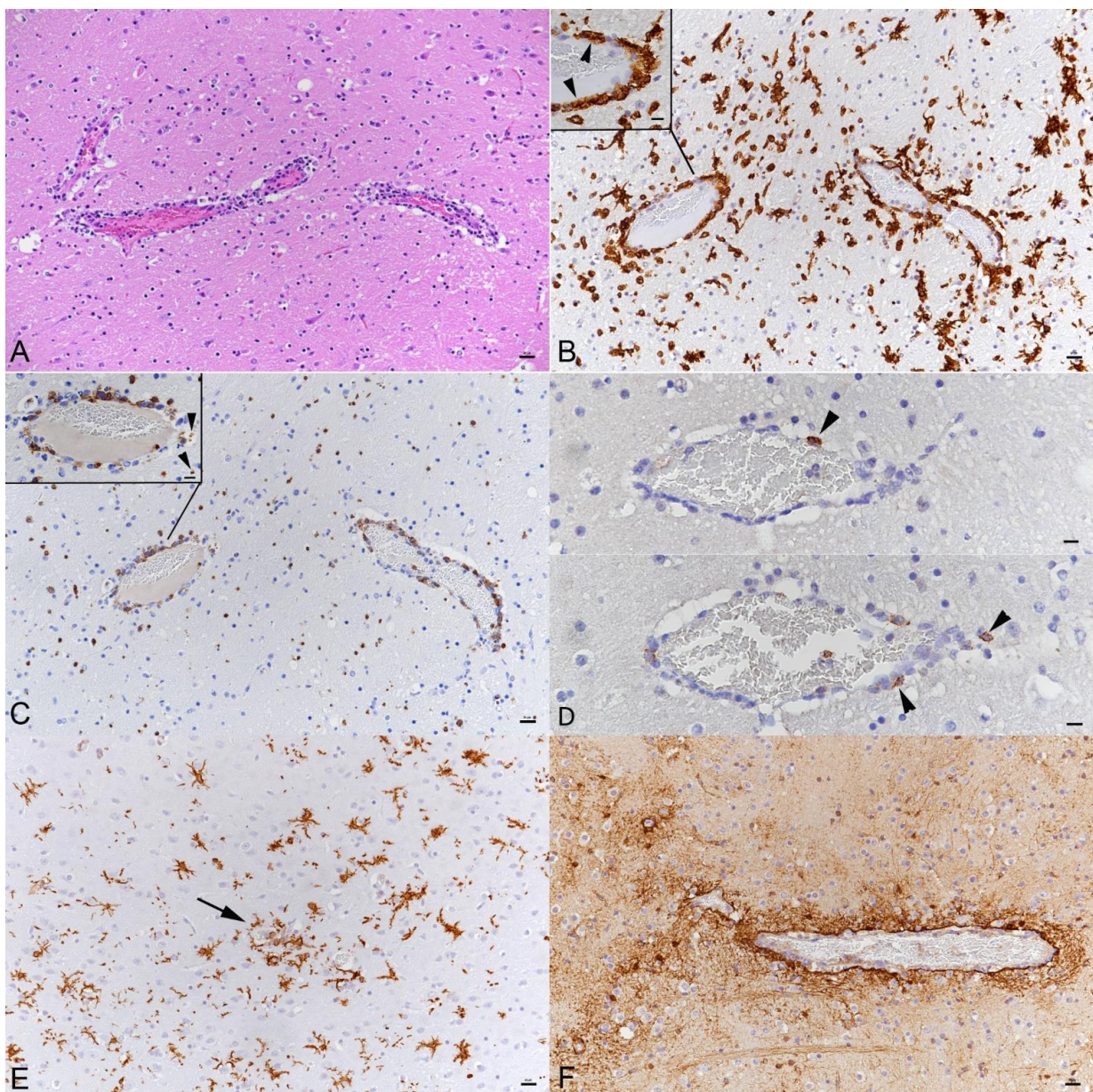


Figure 4. Brain, K18-hACE mouse, day 7 post-intranasal SARS-CoV-2 Pango lineage B infection (10^4 PFU) after initial infection with IAV (10^2 PFU IAV strain A/X31). (A) Brain stem with moderate (peri)vascular leukocyte infiltration and mildly increased cellularity in the parenchyma. HE stain.

(B) Macrophages (Iba1+) dominate in the (peri)vascular infiltrate (inset: arrowheads) and the surrounding parenchyma exhibits microglial activation (Iba1+ stellate shaped cells). (C) T cells (CD3+) are also abundant in the (peri)vascular infiltrates and are found infiltrating the adjacent parenchyma. Inset: vessel with infiltrating T cells; some are degenerate (arrowheads). (D) Neutrophils (Ly6G+; top, arrowhead) and B cells (CD45R/B220+; bottom, arrowheads) are very rare in the infiltrates. (E) Brain stem with activated microglial cells (Iba1+) and small microglial nodule (arrow). (F) Staining of astrocytes (GFAP+) shows hypertrophied astrocytes around a vessel with a mild perivascular infiltrate. (B–F) immunohistochemistry, hematoxylin counterstain. Bars = 20 μ m.

The inflammatory infiltrates were accompanied by moderate diffuse microglial activation/microgliosis in areas with SARS-CoV-2 infected neurons (Figures 4B,E and 5A,B). Microglial nodules were detected mainly adjacent to areas with perivascular infiltrates (Figure 4E). A similar extent of microglial activation and microgliosis was detected at both days 6 and 7 post-infection with any of the variants. In the Delta variant infected mice with brain involvement, infected neurons were accompanied by mild microglial activation and microgliosis in close proximity (Figure 2A,B). Mice infected with the Omicron variant did not show any evidence of microglial activation or microgliosis.

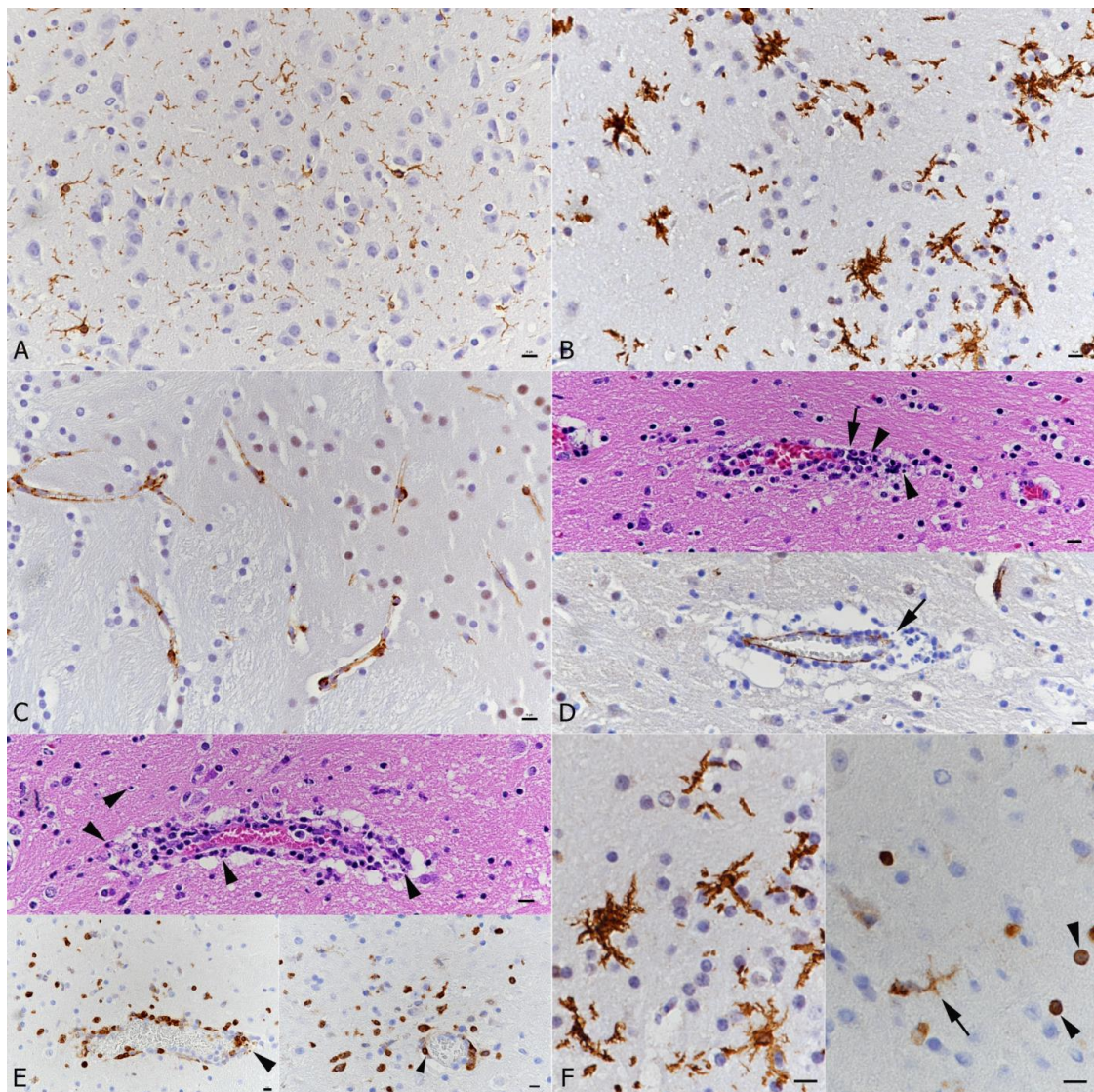


Figure 5. Brain, K18-hACE mice, mock infected and at day 7 post-intranasal SARS-CoV-2 Pango lineage B infection (10^4 PFU) after initial infection with IAV (10^2 PFU IAV strain A/X31). (A) Mock

infected mouse. Quiescent microglia (Iba1+). (B) Infected animal. Diffuse microglial activation (Iba1+ stellate cells). (C) Mock infected mouse. Endothelial cells show cytoplasmic ACE2 expression. (D–F) Infected animal. (D) Vessel with moderate leukocyte infiltration with focal destruction of the vessel wall (arrows) and some degenerate leukocytes (leukocytoclastic component). Top: HE stain; bottom: staining for ACE2, showing disruption of the endothelial cells layer. (E) Vessel with moderate leukocyte infiltration (top: HE stain; bottom: staining for cleaved caspase 3). Individual cells in the infiltrate and in the adjacent parenchyma (top and bottom left: arrowheads) and endothelial cells in an affected vessel (bottom right: arrowhead) undergo apoptosis. (F) Activated microglia (Iba1+; left). Staining for cleaved caspase 3 (right) shows apoptosis of a microglial cell (arrow) and of small round cells (arrowheads; morphology consistent with lymphocytes). (A–E) bars = 20 µm; (F) bars = 10 µm.

There was no evidence of prominent astrogliosis. However, astrocytes immediately adjacent to perivascular infiltrates showed hypertrophy of the cytoplasm consistent with activation (Figure 4F).

3.4. There Is No Evidence of Viral Infection of Glial Cells, Endothelial Cells or Leukocytes or of Neuronal Cell Death, Axonal Damage or Demyelination in Association with SARS-CoV-2 Infection, but of Apoptotic Death of Endothelial Cells and Immune Cells

Despite the widespread infection of neurons, there was no morphological evidence of neuronal cell death. Staining for cleaved caspase 3 did not mark any neurons. Additionally, staining for amyloid precursor protein (APP) to detect disturbances in fast axonal transport as an indicator of acute axonal damage did not show any evidence of the latter. Furthermore, there were no changes indicating obvious demyelination of the white matter. Nevertheless, bilateral and symmetrical myelin sheath vacuolation was detected in the white matter tracts of the pons and the brainstem of animals at 3 and 7 dpi with the Pango lineage B strain, both at low and high doses. Furthermore, mild to moderate vacuolation of the cerebellar white matter without any cellular infiltrates or gliosis was observed. The vacuolation was also present to a mild degree in the animals infected with the Beta strain at 3 dpi, with the Delta strain at 5, 6 and 7 dpi. Capillary endothelial cells which are positive for ACE2 throughout the brain and spinal cord (Figure 5C) were negative in both SARS-CoV-2 IH and ISH. However, in some vessels that exhibited a leukocyte infiltrate, the endothelial layer appeared focally discontinuous (Figure 5D), confirming vasculitis. The infiltrate contained scattered degenerate cells suggesting a leukocytoclastic component. (Figure 5D,E). This was confirmed by staining for cleaved caspase 3; both endothelial cells and leukocytes in the vascular infiltrates were found to be apoptotic. Apoptosis (cleaved caspase 3+) was also observed in a few leukocytes (morphology consistent with lymphocytes) in the adjacent parenchyma (likely infiltrating T cells; Figure 5E) and in occasional microglial cells (Figure 5F). In none of the brains was there any evidence of the SARS-CoV-2 antigen or RNA expression in glial cells.

4. Discussion

COVID-19 is primarily a respiratory disease, with potentially fatal systemic complications that can also involve the CNS. At present, the discussion concerning the pathogenetic and clinical role of encephalopathy in COVID-19 patients is controversial. A variety of mild and/or severe clinical signs have been described, and the reported morphological findings in the brain differ between studies; similarly, the presence and distribution of viral RNA or antigen appears to be inconsistent. Many questions are currently still open regarding the infectious route and spatio-temporal distribution of SARS-CoV-2 in the CNS of COVID-19 patients without comorbidities, confirming the need for appropriate animal models.

In this context, the hACE2 transgenic mouse under the control of the human cytokeratin 18 promoter, a commonly used mouse model to study the pathogenetic effects of SARS-CoV-2 infection, has been employed not only in the present, but also in several other recent studies using the USA-WA1 strain, predominantly at high doses (10^5 to 1.5×10^6 PFU) [26,42,44,54–56]. All these studies, including the present one, show that intranasal inoculation of K18-hACE2 mice with all SARS-CoV-2 variants of concern tested

up to now, but not the Omicron variant, can lead to infection and extensive virus spread in the brain within 5 to 7 days. Infection even stretches into the spinal cord and can basically affect the entire gray matter, including, though only rarely, the cerebellar cortex (Purkinje cells). This indicates that SARS-CoV-2 has no selective neurotropism. Interestingly, we found no evidence of brain involvement with Omicron infections, which would be consistent with the observation made by this and other groups that these strains are less virulent and result in limited infection in K18-hACE2 mice [57]. Omicron variants have a spike protein that differs substantially from that of other variants [58]. It might bind better to ACE2 but less efficiently to whatever the receptor/counter receptor is in neurons.

In the present study, the intranasal inoculation of mice with a low (10^3 PFU) and higher (10^4 PFU) viral dose (compared for the Pango lineage B strain) resulted in variable extents of CNS infection and reached the spinal cord with extensive brain infection. With IAV pre-infection, it was consistently widespread. This does not confirm a direct dose dependence of viral spread, different to what was suspected in other studies [45,55], but suggests some effect of prior damage in the respiratory tract [43]. At the same time, we and others found the virus in the olfactory epithelium and in neurons in the olfactory bulb [42,44,45]. Therefore, a rostral to caudal spread of infection with emphasis on basal structures and consequent infection of cortical areas showing a more patchy than diffuse pattern is most likely. This implies a direct neuronal spread of the virus rather than a hematogenous route of infection, which would likely result in a more disseminated infection pattern as also suggested by other authors [8]. In Delta variant infected mice, viral antigen distribution appeared to have some time-dependent variation. After an increase from 5 to 6 dpi, a decrease in the number of positive neurons seemed to occur from 6 to 7 dpi; this was seen alongside a patchier rather than a diffuse distribution. This could indicate that in these animals the peak of infection was already reached at day 6. However, further studies investigating later time points are required to confirm this observation. Spatio-temporal changes in viral antigen distribution with different virus variants has also been described in another study [45]. An ultrastructural examination on SARS-CoV-2 infected human brain organoids is in agreement with the theory of neuronal spread of the virus, as it provides evidence of virus cell-to-cell-spread between neurons in the organoids [26]. Many of the SARS-CoV-2 antigen positive neurons of mice in this study are located in areas which are secondary or tertiary connections of the olfactory bulb. This gives further evidence of virus entry via the olfactory bulb, as confirmed in both mice [42,56] and humans [10] as a natural route of brain infection by SARS-CoV-2. However, many virus-positive regions that are not directly connected to the olfactory system were also identified, providing further evidence of an additional route of viral dissemination [56].

Clinical signs in mice consistent with neurological disease have rarely been reported, where mice had shown hunched posture, ruffled fur, tremors and ataxic gait from day 4 pi, and died after day 6. These mice carried very high levels of infectious virus in the brain and showed an encephalitis with perivascular hemorrhage. Neuronal death via apoptosis was suspected [44]. Other studies reported perivascular cuffs or vasculitis, neuronal degeneration and necrosis, satellitosis, parenchymal edema, and occasional microthrombi [42,45,54–56], all at day 7 pi. The present study confirms that SARS-CoV-2 variants readily infect neurons in the K18-hACE2 mice, with viral protein accumulation in the entire cytoplasm including the cell processes but does not provide evidence of neuronal cell death in association with infection, indicating that SARS-CoV-2 has no direct cytopathic effect on neurons. This may be due to the lower viral dose, provided that a high viral load would damage neurons directly.

Involvement of the spinal cord, which was a prominent feature in our mouse model, has only been reported in a few human cases [59]. It might be a so far under-recognized neurological complication since neuropathological assessments did not go beyond neuroimaging and the evaluation of several CSF parameters.

Similar to Carossino et al. [42], the present study did not find evidence of demyelination. Clusters of swollen neurons with foamy or vacuolated cytoplasm, occasionally with

pyknotic and eccentric nuclei, as observed by [45], were not detected in our mice. Furthermore, axonal damage was not present in the investigated murine brain sections. However, while both axonal damage and demyelination can occur in COVID-19 patients, they are apparently not common neuropathological findings [18,19,21]. Similar to Vidal et al. [45], we also observed mild spongiosis of tracts of the medulla oblongata in some infected mice, although axons in these tracts were SARS-CoV-2 antigen-negative. The relevance of the vacuolation seen in brain stem and cerebellar white matter, which was most evident in animals infected with the Pango lineage B strain, remains questionable. It also needs to be considered that vacuolation, affecting principally white matter, can be a consequence of prolonged holding of formalin fixed tissue in 70% alcohol, as shown in bovine brains submitted for diagnostic histopathology [60]. This approach, mainly taken to preserve immunoreactivity when processing of the tissue is delayed, was also chosen for the present study; it has the additional advantage that it allows the shipping of tissue which formalin does not. Spongiosis as a common artifact was also described by Wohlsein et al. [61], discussing that it is difficult to discriminate between early significant and non-significant changes.

Neuronal SARS-CoV-2 infection without obvious neuronal degeneration is reminiscent of other neurotropic and persistent viral infections, such as herpes simplex virus (HSV). HSV-1 establishes latency in the mouse model within the earliest stages of acute infection, with the viral genome reaching the neuronal ganglia within the first 24 h of infection [62]. Further studies would now be required to determine whether SARS-CoV-2 also establishes latency or whether there is subsequent neuronal damage.

Viral infection of neurons is evidently associated with an antiviral response in the mice, as indicated by a reported increase in IFN- α mRNA in the brain from day 5 pi onwards, with a peak of both mRNA and protein on day 6 [44]. This is accompanied by an inflammatory response in the brain parenchyma. Similar to a previous study [54], we observed a mild non-suppurative, macrophage and T cell driven encephalitis (perivascular infiltrates and occasional vasculitis) in all mice that harbored the viral antigen in the brains at 6 and 7 dpi. This appeared to be slightly more intense with more extensive neuronal virus antigen expression in animals that had been pre-infected with IAV, suggesting easier access to the brain with pre-existing damage due to IAV infection [43]. Transcriptional investigations also confirmed the inflammatory state of the brain, demonstrating an increase in inflammatory cytokines and chemokines (IL-6, TNF- α , IFN- γ , IL-1 β , MIP-1 α , MIP-2, IP-10) in the brain of infected mice [44,55]. This might also explain the activation/hypertrophy of astrocytes in areas with perivascular infiltrates and the diffuse microglial activation and multifocal microgliosis that we and others observed [42,55,63]. Both glial cell populations are responsive to proinflammatory signals from endothelial cells, macrophages and/or neurons [6]. The proinflammatory gene expression program initiated after viral infection would expand neuroinflammation [28]. Interestingly, microgliosis was also shown in the olfactory bulb of infected mice without obvious inflammatory cell infiltration similar to human patients [20]. Activated microglia may itself undergo a phenotypic shift and display exaggerated release of pro-inflammatory mediators and aberrant phagocytic activity, inducing neurodegeneration [64]. This could explain the diffuse astrogliosis reported from other mouse and human studies [9,42,45] as well as neuronophagia by microglial cells, which was seen in some human COVID-19 patients [23] and one mouse study [42].

In previous studies, we and others have shown that IAV pre-infection of K18-hACE2 mice results in more severe SARS-CoV-2-associated pulmonary changes and higher amounts of infectious virus at 6 or 7 days post-Pango lineage B infection [43,65]. Interestingly though, viral loads in the brain were not found to be increased [65], although we observed more widespread brain infection in animals that were infected with IAV. It is currently unclear which direct impact IAV infection has for the subsequent SARS-CoV-2 challenge, but more efficient virus entry could be an option, since IAV infection was shown to upregulate ACE2 expression in vitro [65]. In co-infected hamsters, an involvement of IL-6 in the increased severity of pneumonia was discussed [66].

While we did not find evidence of neuronal death, we observed apoptosis of infiltrating lymphocytes, capillary endothelial cells and macrophages/microglial cells in proximity to perivascular infiltrates. As in a previous study [42], none of these cells were found to be SARS-CoV-2 infected. This result is in line with recent findings in SARS-CoV-2 infected human brain organoids, which provided evidence that infected neurons do not die but can promote the death of adjacent uninfected cells [26]. Using single cell RNA sequencing, the study showed that SARS-CoV-2 infected cells in the organoids were in a hypermetabolic state, whereas uninfected cells nearby were in a catabolic state and a hypoxic environment, as shown by HIF1 α expression [26]. The same may be true for the brain of K18-hACE2 mice with widespread neuronal SARS-CoV-2 infection. Additionally, coupled proliferation and apoptosis are assumed to maintain the quite rapid turnover of microglia in the adult brain [67]. We did not determine the proliferation rate in this study, but such “physiological” turnover should be considered when interpreting microglial apoptosis in SARS-CoV-2 infected mice. In another hACE2 mouse study, with prominent microglial activation, pro-inflammatory CSF cytokines/chemokines were elevated for at least 7 weeks post-infection, a feature also reported in human patients with long COVID syndrome [68]. Moreover, *in vitro* neuronal cell cultures of K18-hACE2 mouse neurons showed an upregulation of the expression of genes involved in innate immunity and inflammation [69]. An astrocytic SARS-CoV-2 infection, which was described in human brains and cultured astrocytes [36], could not be detected in any mouse brain with any virus variant in our study. Therefore, the present study found no evidence that SARS-CoV-2 infects astrocytes. Nevertheless, due to the controversial findings further studies are needed to elucidate the role of astrocytes in SARS-CoV-2 infection.

Several morphological changes in the mice used in the present study recapitulate findings reported in brains of human COVID-19 patients, such as mild perivascular inflammatory infiltrates [21] and microgliosis [20]. Further vascular lesions, apart from vasculitis/endotheliitis, such as ischemic infarcts [18,26] or microthrombi [16], that seem to be frequent in fatal human COVID-19 cases, are obviously not a regular feature in this mouse model since only two studies reported occasional microthrombi in the brain [55,56]. This could be due to the lack of endothelial cell infection in the brain of the mice, whereas it was seen in association with fresh ischemic infarcts in the brain of a COVID-19 patient [10,26]. In our study, mice infected with the delta variant did not show inflammatory changes but needed to be euthanized due to clinical symptoms. Interestingly, the presence of the virus in the brain of the human patients is apparently also not consistently associated with leukocyte infiltration, indicating that SARS-CoV-2 does not necessarily induce an immune response similar to other neurotropic viruses [26].

The main host receptor for SARS-CoV-2 is the human angiotensin-converting enzyme 2 (hACE2). While a study of the brain of fatal human COVID-19 cases showed ACE2 expression in cortical neurons and found evidence that ACE2 is required for infection of human brain organoids [26], neuroinvasion and spread in the K18-hACE2 mice is apparently not directly dependent upon ACE2 expression because the virus does not infect all ACE2-expressing cells and does infect cells without apparent ACE2 expression [42]. Indeed, in line with the findings of previous studies, we only detected ACE2 protein expression in capillary endothelial cells, ependymal cells and choroid plexus epithelium in the brain and spinal cord, in the absence of detectable viral antigen [26,42,43]. In human COVID-19 patients, viral particles were detected in the endothelium of capillaries in the kidney, liver, heart, lung and small intestine. This was associated with an endotheliitis [70]. This finding was controversial [14]. Furthermore, ultrastructural examination of the brain of one human patient showed viral particles in small vesicles of endothelial cells, suspecting an additional hematogenous route of brain infection [12]. Indeed, using intravenously injected radioiodinated SARS-CoV-2 S1 has shown that the viral protein can cross the BBB, and likely by absorptive transcytosis [34]. Hence, it may be due to the fact that endothelial ACE2 expression in the K18-hACE2 mice represents only the murine protein [42] that the

brain endothelium of the mice does not become infected by SARS-CoV-2. The role of other receptors is still a subject of debate; a possible candidate might be neuropilin-1 [8].

Based on current knowledge, it seems likely that in COVID-19 patients, the virus can access the brain in several ways. In severe COVID-19, viremia could allow access to the brain via the vasculature [71]. With the platelet hyperactivity in critically ill patients [72] and abnormal blood clotting or unusual thrombotic presentations [73,74], this might lead to the ischemic changes described in a proportion of fatal cases, without the viral infection of neurons. This might not be mirrored by the murine model as viremia may not occur [55]. In mild COVID-19, i.e., without viremia, infection of the brain via the olfactory bulb and other possible neurogenic routes could occur. This would then lead to exclusive neuronal infection and only a mild inflammatory response. It might be this scenario that explains the loss of taste and smell and severe headaches reported in patients with mild disease. Nevertheless, infection (and consecutive degeneration) of non-neuronal cell populations in the olfactory mucosa, such as sustentacular cells, was considered a main contributing factor to anosmia [11,75]. In contrast to our murine study, hamsters and humans did not show the viral antigen in the olfactory bulb [11,75,76].

The murine model does not fulfil all morphological criteria of acute human neurological COVID-19. However, brain infection following a lower dose of intranasal challenge might represent a mouse model for long COVID-19 syndrome studies. The pathogenesis of this sequel of the acute disease is still unknown, but fatigue, muscle aches, breathlessness and headaches are the most frequently reported symptoms [77,78]. A persistent low-grade smoldering inflammatory response to newly budding virions might be central to the condition. In addition, the degeneration or impaired function of neuronal and glial cells that are cardinal for the physiological function of the brain might be an option [79]. A mild inadequate immune response with persistent viral load and viral evasion of the immune surveillance are suspected key factors [79]. This is supported by the fact that COVID-19 patients still exhibit a significant remaining inflammatory response in the serum between 40 and 60 days post-infection [80]. Further investigations of the inflammatory response at the transcriptome and translational level in the murine model could provide further insights.

These data also have important implications for the development of therapeutic interventions. Firstly, the endothelium and astrocyte foot processes represent key components of the BBB, protecting the brain from the accumulation of endo- and xeno-biotics. Future studies should address the consequences of infection for maintenance of barrier integrity to mitigate potential inadvertent delivery of neurotoxic agents that would otherwise not permeate the brain. Secondly, several studies have already sought to understand the pulmonary distribution of postulated therapeutic interventions [81–83] but robust efficacy of antivirals and/or immunomodulatory agents may also necessitate adequate exposure within the CNS. Notably, the repurposed antivirals remdesivir, favipiravir and molnupiravir exhibit low concentrations in the brain relative to plasma in preclinical species [84–87]. Furthermore, dexamethasone also exhibits low brain penetration in mice with an intact BBB, but this increases in mice genetically engineered to be missing a critical drug transporter, P-glycoprotein [88]. Further work is required to define the importance of brain penetration of therapeutics being investigated as interventions across the spectrum of disease from prevention, mild, moderate, severe to long COVID-19.

5. Conclusions

Despite widespread neuronal infection, pathomorphological changes of the course of disease consisted of mild lymphohistiocytic inflammation and microglial activation. Only neuronal cells were infected, which supported the infectious route via the olfactory epithelium, olfactory bulb and transsynaptic spreading. The limited expression of ACE2 raises the question for ACE2-independent pathogenetic mechanisms to explain the neurotropism of the virus. Microgliosis and immune cell apoptosis were the main pathological features in our study indicating a potential important role of microglial cells in the pathogenesis of neuromanifestation in COVID-19.

Supplementary Materials: The following are available online at <https://www.mdpi.com/article/10.3390/v14051020/s1>, Table S1: Antibodies and detection methods used for immunohistochemistry. Figure S1: Infection of K18-hACE2 mice with SARS-CoV-2 VOCs leads to substantial weight loss. Figure S2: Infection of K18-hACE2 mice with SARS-CoV-2 VOCs leads to extensive pulmonary infection and spreads to the brain.

Author Contributions: Conceptualization, J.P.S. and A.K. (Anja Kipar); methodology, F.S., J.J.C., P.S., E.G.B., A.K. (Adam Kirby), K.S., S.W.-G., G.L.H., E.I.P., B.D.M., A.O., J.A.H., J.P.S. and A.K. (Anja Kipar); formal analysis, F.S., J.J.C., J.P.S. and A.K. (Anja Kipar); investigation, F.S., J.J.C., P.S., E.G.B., A.K. (Adam Kirby), K.S., G.L.H., E.I.P., B.D.M., A.O., J.A.H., J.P.S. and A.K. (Anja Kipar); resources, J.P.S. and A.K. (Anja Kipar); writing—original draft preparation, F.S., J.P.S. and A.K. (Anja Kipar); writing—review and editing, F.S., J.J.C., P.S., K.S., G.L.H., E.I.P., B.D.M., A.O., J.A.H., J.P.S. and A.K. (Anja Kipar); funding acquisition, A.O., J.A.H. and J.P.S. All authors have read and agreed to the published version of the manuscript.

Funding: This work was funded in part by the US Food and Drug Administration (USA) 75F40120C00085, Characterization of severe coronavirus infection in humans and model systems for medical countermeasure development and evaluation. Work in the laboratory is also supported by the MRC grant MR/W005611/1, G2P-UK; A National Virology Consortium to address phenotypic consequences of SARS-CoV-2 genomic variation. B.D.M. is supported to conduct COVID-19 neuroscience research by the UKRI/MRC (MR/V03605X/1) and for additional neurological inflammation research due to viral infection from the MRC/UKRI (MR/V007181/1), MRC (MR/T028750/1) and Wellcome (ISSF201902/3).

Institutional Review Board Statement: Animal work was approved by the local University of Liverpool Animal Welfare and Ethical Review Body and performed under the UK Home Office Project Licence PP4715265. See also Materials and Methods.

Informed Consent Statement: Not applicable.

Acknowledgments: We are grateful to the technical staff in the Histology Laboratory, Institute of Veterinary Pathology, Vetsuisse Faculty, University of Zurich (IVPZ), for excellent technical support.

Conflicts of Interest: The authors declare no conflict of interest.

References

1. Bernard-Valnet, R.; Pizzarotti, B.; Anichini, A.; Demars, Y.; Russo, E.; Schmidhauser, M.; Cerutti-Sola, J.; Rossetti, A.O.; Du Pasquier, R. Two patients with acute meningoencephalitis concomitant with SARS-CoV-2 infection. *Eur. J. Neurol.* **2020**, *27*, e43–e44. [[CrossRef](#)] [[PubMed](#)]
2. Helms, J.; Kremer, S.; Merdji, H.; Clere-Jehl, R.; Schenck, M.; Kummerlen, C.; Collange, O.; Boulay, C.; Fafi-Kremer, S.; Ohana, M.; et al. Neurologic features in severe SARS-CoV-2 infection. *N. Engl. J. Med.* **2020**, *382*, 2268–2270. [[CrossRef](#)] [[PubMed](#)]
3. Huang, Y.H.; Jiang, D.; Huang, J.T. SARS-CoV-2 detected in cerebrospinal fluid by PCR in a case of COVID-19 encephalitis. *Brain Behav. Immun.* **2020**, *87*, 149. [[CrossRef](#)] [[PubMed](#)]
4. Mao, L.; Jin, H.; Wang, M.; Hu, Y.; Chen, S.; He, Q.; Chang, J.; Hong, C.; Zhou, Y.; Wang, D.; et al. Neurologic Manifestations of Hospitalized Patients With Coronavirus Disease 2019 in Wuhan, China. *JAMA Neurol.* **2020**, *77*, 683–690. [[CrossRef](#)] [[PubMed](#)]
5. Moriguchi, T.; Harii, N.; Goto, J.; Harada, D.; Sugawara, H.; Takamino, J.; Ueno, M.; Sakata, H.; Kondo, K.; Myose, N.; et al. A first case of meningitis/encephalitis associated with SARS-Coronavirus-2. *Int. J. Infect. Dis.* **2020**, *94*, 55–58. [[CrossRef](#)]
6. Oxley, T.J.; Mocco, J.; Majidi, S.; Kellner, C.P.; Shoirah, H.; Singh, I.P.; De Leacy, R.A.; Shigematsu, T.; Ladner, T.R.; Yaeger, K.A.; et al. Large-vessel stroke as a presenting feature of COVID-19 in the young. *N. Engl. J. Med.* **2020**, *382*, e60. [[CrossRef](#)] [[PubMed](#)]
7. Poyiadji, N.; Shahin, G.; Noujaim, D.; Stone, M.; Patel, S.; Griffith, B. COVID-19-associated acute hemorrhagic necrotizing encephalopathy: Imaging features. *Radiology* **2020**, *296*, E119–E120. [[CrossRef](#)]
8. Cantuti-Castelvetri, L.; Ojha, R.; Pedro, L.D.; Djannatian, M.; Franz, J.; Kuivanen, S.; van der Meer, F.; Kallio, K.; Kaya, T.; Anastasina, M.; et al. Neuropilin-1 facilitates SARS-CoV-2 cell entry and infectivity. *Science* **2020**, *370*, 856–860. [[CrossRef](#)]
9. Matschke, J.; Lütgehetmann, M.; Hagel, C.; Sperhake, J.P.; Schröder, A.S.; Edler, C.; Mushumba, H.; Fitzek, A.; Allweiss, L.; Dandri, M.; et al. Neuropathology of patients with COVID-19 in Germany: A post-mortem case series. *Lancet Neurol.* **2020**, *19*, 919–929. [[CrossRef](#)]
10. Meinhardt, J.; Radke, J.; Dittmayer, C.; Franz, J.; Thomas, C.; Mothes, R.; Laue, M.; Schneider, J.; Brünink, S.; Greuel, S.; et al. Olfactory transmucosal SARS-CoV-2 invasion as a port of central nervous system entry in individuals with COVID-19. *Nat. Neurosci.* **2021**, *24*, 168–175. [[CrossRef](#)]

11. Khan, M.; Yoo, S.J.; Clijsters, M.; Backaert, W.; Vanstapel, A.; Speleman, K.; Lietaer, C.; Choi, S.; Hether, T.D.; Marcelis, L.; et al. Visualizing in deceased COVID-19 patients how SARS-CoV-2 attacks the respiratory and olfactory mucosae but spares the olfactory bulb. *Cell* **2021**, *184*, 5932–5949.e15. [[CrossRef](#)]
12. Paniz-Mondolfi, A.; Bryce, C.; Grimes, Z.; Gordon, R.E.; Reidy, J.; Lednicky, J.; Sordillo, E.M.; Fowkes, M. Central nervous system involvement by severe acute respiratory syndrome coronavirus-2 (SARS-CoV-2). *J. Med. Virol.* **2020**, *92*, 699–702. [[CrossRef](#)] [[PubMed](#)]
13. Al-Sarraj, S.; Troakes, C.; Hanley, B.; Osborn, M.; Richardson, M.P.; Hotopf, M.; Bullmore, E.; Everall, I.P. Invited Review: The spectrum of neuropathology in COVID-19. *Neuropathol. Appl. Neurobiol.* **2021**, *47*, 3–16. [[CrossRef](#)] [[PubMed](#)]
14. Goldsmith, C.S.; Miller, S.E.; Martines, R.B.; Bullock, H.A.; Zaki, S.R. Electron microscopy of SARS-CoV-2: A challenging task. *Lancet* **2020**, *395*, e99. [[CrossRef](#)]
15. Deigendesch, N.; Sironi, L.; Kutza, M.; Wischnewski, S.; Fuchs, V.; Hench, J.; Frank, A.; Nienhold, R.; Mertz, K.D.; Cathomas, G.; et al. Correlates of critical illness-related encephalopathy predominate postmortem COVID-19 neuropathology. *Acta Neuropathol.* **2020**, *140*, 583–586. [[CrossRef](#)]
16. Fabbri, V.P.; Foschini, M.P.; Lazzarotto, T.; Gabrielli, L.; Cenacchi, G.; Gallo, C.; Aspide, R.; Frascaroli, G.; Cortelli, P.; Riefolo, M.; et al. Brain ischemic injury in COVID-19-infected patients: A series of 10 post-mortem cases. *Brain Pathol.* **2021**, *31*, 205–210. [[CrossRef](#)]
17. Jaunmuktane, Z.; Mahadeva, U.; Green, A.; Sekhawat, V.; Barrett, N.A.; Childs, L.; Shankar-Hari, M.; Thom, M.; Jäger, H.R.; Brandner, S. Microvascular injury and hypoxic damage: Emerging neuropathological signatures in COVID-19. *Acta Neuropathol.* **2020**, *140*, 397–400. [[CrossRef](#)]
18. Kantonen, J.; Mahzabin, S.; Mäyränpää, M.I.; Tynneninen, O.; Paetau, A.; Andersson, N.; Sajantila, A.; Vapalahti, O.; Carpén, O.; Kekäläinen, E.; et al. Neuropathologic features of four autopsied COVID-19 patients. *Brain Pathol.* **2020**, *30*, 1012–1016. [[CrossRef](#)]
19. Reichard, R.R.; Kashani, K.B.; Boire, N.A.; Constantopoulos, E.; Guo, Y.; Lucchinetti, C.F. Neuropathology of COVID-19: A spectrum of vascular and acute disseminated encephalomyelitis (ADEM)-like pathology. *Acta Neuropathol.* **2020**, *140*, 1–6. [[CrossRef](#)]
20. Schurink, B.; Roos, E.; Radonic, T.; Barbe, E.; Bouman, C.S.C.; de Boer, H.H.; de Bree, G.J.; Bulle, E.B.; Aronica, E.M.; Florquin, S.; et al. Viral presence and immunopathology in patients with lethal COVID-19: A prospective autopsy cohort study. *Lancet Microbe* **2020**, *1*, e290–e299. [[CrossRef](#)]
21. Solomon, I.H.; Normandin, E.; Bhattacharyya, S.; Mukerji, S.S.; Keller, K.; Ali, A.S.; Adams, G.; Hornick, J.L.; Padera, R.F., Jr.; Sabeti, P. Neuropathological features of Covid-19. *N. Engl. J. Med.* **2020**, *383*, 989–992. [[CrossRef](#)] [[PubMed](#)]
22. von Weyhern, C.H.; Kaufmann, I.; Neff, F.; Kremer, M. Early evidence of pronounced brain involvement in fatal COVID-19 outcomes. *Lancet* **2020**, *395*, e109. [[CrossRef](#)]
23. Al-Dalahmah, O.; Thakur, K.T.; Nordvig, A.S.; Prust, M.L.; Roth, W.; Lignelli, A.; Uhlemann, A.C.; Miller, E.H.; Kunnath-Velayudhan, S.; Del Portillo, A.; et al. Neuronophagia and microglial nodules in a SARS-CoV-2 patient with cerebellar hemorrhage. *Acta Neuropathol. Commun.* **2020**, *8*, 147. [[CrossRef](#)] [[PubMed](#)]
24. Bussani, R.; Schneider, E.; Zentilin, L.; Collesi, C.; Ali, H.; Braga, L.; Volpe, M.C.; Colliva, A.; Zanconati, F.; Berlot, G.; et al. Persistence of viral RNA, pneumocyte syncytia and thrombosis are hallmarks of advanced COVID-19 pathology. *EBioMedicine* **2020**, *61*, 103104. [[CrossRef](#)]
25. Puelles, V.G.; Lütgehetmann, M.; Lindenmeyer, M.T.; Sperhake, J.P.; Wong, M.N.; Allweiss, L.; Chilla, S.; Heinemann, A.; Wanner, N.; Liu, S.; et al. Multiorgan and renal tropism of SARS-CoV-2. *N. Engl. J. Med.* **2020**, *383*, 590–592. [[CrossRef](#)]
26. Song, E.; Zhang, C.; Israelow, B.; Lu-Culligan, A.; Prado, A.V.; Skriabine, S.; Lu, P.; Weizman, O.E.; Liu, F.; Dai, Y.; et al. Neuroinvasion of SARS-CoV-2 in human and mouse brain. *J. Exp. Med.* **2021**, *218*, e20202135. [[CrossRef](#)]
27. Najjar, S.; Najjar, A.; Chong, D.J.; Pramanik, B.K.; Kirsch, C.; Kuzniecky, R.I.; Pacia, S.V.; Azhar, S. Central nervous system complications associated with SARS-CoV-2 infection: Integrative concepts of pathophysiology and case reports. *J. Neuroinflamm.* **2020**, *17*, 231. [[CrossRef](#)]
28. Murta, V.; Villarreal, A.; Ramos, A.J. Severe Acute Respiratory Syndrome Coronavirus 2 impact on the central nervous system: Are astrocytes and microglia main players or merely bystanders? *ASN Neuro* **2020**, *12*, 1759091420954960. [[CrossRef](#)]
29. Vargas, G.; Medeiros Geraldo, L.H.; Gedeão Salomão, N.; Viana Paes, M.; Regina Souza Lima, F.; Carvalho Alcantara Gomes, F. Severe acute respiratory syndrome coronavirus 2 (SARS-CoV-2) and glial cells: Insights and perspectives. *Brain Behav. Immun. Health* **2020**, *7*, 100127. [[CrossRef](#)]
30. Perry, V.H.; Cunningham, C.; Holmes, C. Systemic infections and inflammation affect chronic neurodegeneration. *Nat. Rev. Immunol.* **2007**, *7*, 161–167. [[CrossRef](#)]
31. Perry, V.H.; Teeling, J. Microglia and macrophages of the central nervous system: The contribution of microglia priming and systemic inflammation to chronic neurodegeneration. *Semin. Immunopathol.* **2013**, *35*, 601–612. [[CrossRef](#)] [[PubMed](#)]
32. Murta, V.; Fariás, M.I.; Pitossi, F.J.; Ferrari, C.C. Chronic systemic IL-1 β exacerbates central neuroinflammation independently of the blood-brain barrier integrity. *J. Neuroimmunol.* **2015**, *278*, 30–43. [[CrossRef](#)] [[PubMed](#)]
33. Swanson, P.A., II; McGavern, D.B. Viral diseases of the central nervous system. *Curr. Opin. Virol.* **2015**, *11*, 44–54. [[CrossRef](#)] [[PubMed](#)]
34. Rhea, E.M.; Logsdon, A.F.; Hansen, K.M.; Williams, L.M.; Reed, M.J.; Baumann, K.K.; Holden, S.J.; Raber, J.; Banks, W.A.; Erickson, M.A. The S1 protein of SARS-CoV-2 crosses the blood-brain barrier in mice. *Nat. Neurosci.* **2020**, *24*, 368–378. [[CrossRef](#)]

35. Michael, B.D.; Bricio-Moreno, L.; Sorensen, E.W.; Miyabe, Y.; Lian, J.; Solomon, T.; Kurt-Jones, E.A.; Luster, A.D. Astrocyte- and neuron-derived CXCL1 drives neutrophil transmigration and blood-brain barrier permeability in viral encephalitis. *Cell Rep.* **2020**, *32*, 108150. [CrossRef] [PubMed]
36. Crunfli, F.; Carregari, V.C.; Veras, F.P.; Vendramini, P.H.; Valença, A.G.F.; Antunes, A.S.L.M.; Brandão-Teles, C.; da Silva Zuccoli, G.; Reis-de-Oliveira, G.; Silva-Costa, L.C.; et al. Morphological, cellular and molecular basis of brain infection in COVID-19 patients. *medRxiv* **2022**. preprint. [CrossRef]
37. Alam, S.B.; Willows, S.; Kulka, M.; Sandhu, J.K. Severe acute respiratory syndrome coronavirus 2 may be an underappreciated pathogen of the central nervous system. *Eur. J. Neurol.* **2020**, *27*, 2348–2360. [CrossRef]
38. Mahalaxmi, I.; Kaavya, J.; Mohana Devi, S.; Balachandar, V. COVID-19 and olfactory dysfunction: A possible associative approach towards neurodegenerative diseases. *J. Cell Physiol.* **2021**, *236*, 763–770. [CrossRef]
39. Lavi, E.; Cong, L. Type I astrocytes and microglia induce a cytokine response in an encephalitic murine coronavirus infection. *Exp. Mol. Pathol.* **2020**, *115*, 104474. [CrossRef]
40. Hoffmann, M.; Kleine-Weber, H.; Schroeder, S.; Kruger, N.; Herrler, T.; Erichsen, S.; Schiergens, T.S.; Herrler, G.; Wu, N.H.; Nitsche, A.; et al. SARS-CoV-2 cell entry depends on ACE2 and TMPRSS2 and is blocked by a clinically proven protease inhibitor. *Cell* **2020**, *181*, 271–280.e278. [CrossRef]
41. McCray, P.B., Jr.; Pewe, L.; Wohlford-Lenane, C.; Hickey, M.; Manzel, L.; Shi, L.; Netland, J.; Jia, H.P.; Halabi, C.; Sigmund, C.D.; et al. Lethal infection of K18-hACE2 mice infected with severe acute respiratory syndrome coronavirus. *J. Virol.* **2007**, *81*, 813–821. [CrossRef] [PubMed]
42. Carossino, M.; Kenney, D.; O'Connell, A.K.; Montanaro, P.; Tseng, A.E.; Gertje, H.P.; Grosz, K.A.; Ericsson, M.; Huber, B.R.; Kurnick, S.A.; et al. Fatal Neurodissemination and SARS-CoV-2 Tropism in K18-hACE2 Mice Is Only Partially Dependent on hACE2 Expression. *Viruses* **2022**, *14*, 535. [CrossRef] [PubMed]
43. Clark, J.J.; Penrice-Randal, R.; Sharma, P.; Kipar, A.; Dong, X.; Davidson, A.; Kavanagh Williamson, M.; Matthews, D.A.; Turtle, L.; Prince, T.; et al. Sequential infection with influenza A virus followed by severe acute respiratory syndrome coronavirus 2 (SARS-CoV-2) leads to more severe disease and encephalitis in a mouse model of COVID-19. *bioRxiv* **2021**. preprint. [CrossRef]
44. Kumari, P.; Rothan, H.A.; Natekar, J.P.; Stone, S.; Pathak, H.; Strate, P.G.; Arora, K.; Brinton, M.A.; Kumar, M. Neuroinvasion and encephalitis following intranasal inoculation of SARS-CoV-2 in K18-hACE2 mice. *Viruses* **2021**, *13*, 132. [CrossRef]
45. Vidal, E.; López-Figueroa, C.; Rodon, J.; Pérez, M.; Brustolin, M.; Cantero, G.; Guallar, V.; Izquierdo-Useros, N.; Carrillo, J.; Blanco, J.; et al. Chronological brain lesions after SARS-CoV-2 infection in hACE2-transgenic mice. *Vet. Pathol.* **2021**. online ahead of print. [CrossRef]
46. Patterson, E.I.; Prince, T.; Anderson, E.R.; Casas-Sanchez, A.; Smith, S.L.; Cansado-Utrilla, C.; Solomon, T.; Griffiths, M.J.; Acosta-Serrano, Á.; Turtle, L.; et al. Methods of inactivation of SARS-CoV-2 for downstream biological assays. *J. Infect. Dis.* **2020**, *222*, 1462–1467. [CrossRef]
47. Cele, S.; Gazy, I.; Jackson, L.; Hwa, S.H.; Tegally, H.; Lustig, G.; Giandhari, J.; Pillay, S.; Wilkinson, E.; Naidoo, Y.; et al. Escape of SARS-CoV-2 501Y.V2 from neutralization by convalescent plasma. *Nature* **2021**, *593*, 142–146. [CrossRef]
48. Dejnirattisai, W.; Shaw, R.H.; Supasa, P.; Liu, C.; Stuart, A.S.; Pollard, A.J.; Liu, X.; Lambe, T.; Crook, D.; Stuart, D.I.; et al. Reduced neutralisation of SARS-CoV-2 omicron B.1.1.529 variant by post-immunisation serum. *Lancet* **2022**, *399*, 234–236. [CrossRef]
49. Bentley, E.G.; Kirby, A.; Sharma, P.; Kipar, A.; Mega, D.F.; Bramwell, C.; Penrice-Randal, R.; Prince, T.; Brown, J.C.; Zhou, J.; et al. SARS-CoV-2 Omicron-B.1.1.529 Variant leads to less severe disease than Pango B and Delta variants strains in a mouse model of severe COVID-19. *bioRxiv* **2021**. preprint. [CrossRef]
50. Salzer, R.; Clark, J.J.; Vaysburd, M.; Chang, V.T.; Albecka, A.; Kiss, L.; Sharma, P.; Gonzalez Llamazares, A.; Kipar, A.; Hiscox, J.A.; et al. Single-dose immunisation with a multimerised SARS-CoV-2 receptor binding domain (RBD) induces an enhanced and protective response in mice. *FEBS Lett.* **2021**, *595*, 2323–2340. [CrossRef]
51. Salguero, F.J.; White, A.D.; Slack, G.S.; Fotheringham, S.A.; Bewley, K.R.; Gooch, K.E.; Longet, S.; Humphries, H.E.; Watson, R.J.; Hunter, L.; et al. Comparison of rhesus and cynomolgus macaques as an infection model for COVID-19. *Nat. Commun.* **2021**, *12*, 1260. [CrossRef] [PubMed]
52. Saura-Martinez, H.; Al-Saadi, M.; Stewart, J.P.; Kipar, K. Sheep-associated malignant catarrhal fever: Role of latent virus and macrophages in vasculitis. *Vet. Pathol.* **2021**, *58*, 332–345. [CrossRef] [PubMed]
53. 3d Viewer: Allen Brain Atlas: Mouse Connectivity. Available online: <https://connectivity.brain-map.org/3d-viewer?v=1&types=PLY&PLY=453%2C1057%2C31%2C44%2C254%2C500%2C922%2C895%2C549%2C1097%2C386%2C370%2C1132%2C987%2C669%2C1089%2C672%2C502%2C909%2C961%2C972%2C507> (accessed on 8 March 2022).
54. Oladunni, F.S.; Park, J.G.; Pino, P.A.; Gonzalez, O.; Akhter, A.; Allué-Guardia, A.; Olmo-Fontánez, A.; Gautam, S.; Garcia-Vilanova, A.; Ye, C.; et al. Lethality of SARS-CoV-2 infection in K18 human angiotensin-converting enzyme 2 transgenic mice. *Nat. Commun.* **2020**, *11*, 6122. [CrossRef] [PubMed]
55. Yinda, C.K.; Port, J.R.; Bushmaker, T.; Offei Owusu, I.; Purushotham, J.N.; Avanzato, V.A.; Fischer, R.J.; Schulz, J.E.; Holbrook, M.G.; Hebner, M.J.; et al. K18-hACE2 mice develop respiratory disease resembling severe COVID-19. *PLoS Pathog.* **2021**, *17*, e1009195. [CrossRef]
56. Zheng, J.; Wong, L.Y.R.; Li, K.; Verma, A.K.; Ortiz, M.E.; Wohlford-Lenane, C.; Leidinger, M.R.; Knudson, C.M.; Meyerholz, D.K.; McCray, P.B.; et al. COVID-19 treatments and pathogenesis including anosmia in K18-hACE2 mice. *Nature* **2021**, *589*, 603–607. [CrossRef]

57. Halfmann, P.J.; Iida, S.; Iwatsuki-Horimoto, K.; Maemura, T.; Kiso, M.; Scheaffer, S.M.; Darling, T.L.; Joshi, A.; Loeber, S.; Singh, G.; et al. SARS-CoV-2 Omicron virus causes attenuated disease in mice and hamsters. *Nature* **2022**, *603*, 687–692. [[CrossRef](#)]
58. Alkhatib, M.; Salpini, R.; Carioti, L.; Ambrosio, F.A.; D’Anna, S.; Duca, L.; Costa, G.; Bellocchi, M.C.; Piermatteo, L.; Artese, A.; et al. Update on SARS-CoV-2 Omicron Variant of Concern and Its Peculiar Mutational Profile. *Microbiol. Spectr.* **2022**, *10*, e0273221. [[CrossRef](#)]
59. Mondal, R.; Deb, S.; Shome, G.; Ganguly, U.; Lahiri, D.; Leon, J.B. Spectrum of spinal cord involvement in COVID-19: A systematic review. *medRxiv* **2020**. preprint. [[CrossRef](#)]
60. Wells, G.A.; Wells, M. Neuropil vacuolation in brain: A reproducible histological processing artefact. *J. Comp. Pathol.* **1989**, *101*, 355–362. [[CrossRef](#)] [[PubMed](#)]
61. Wohlsein, P.; Deschl, U.; Baumgärtner, W. Nonlesions, unusual cell types, and postmortem artifacts in the central nervous system of domestic animals. *Vet. Pathol.* **2013**, *50*, 122–143. [[CrossRef](#)]
62. Steiner, I.; Spivack, J.G.; Deshmane, S.L.; Ace, C.I.; Preston, C.M.; Fraser, N.W. A herpes simplex virus type 1 mutant containing a nontransducing Vmw65 protein establishes latent infection in vivo in the absence of viral replication and reactivates efficiently from explanted trigeminal ganglia. *J. Virol.* **1990**, *64*, 1630–1638. [[CrossRef](#)] [[PubMed](#)]
63. Winkler, E.S.; Bailey, A.L.; Kafai, N.M.; Nair, S.; McCune, B.T.; Yu, J.; Fox, J.M.; Chen, R.E.; Earnest, J.T.; Keeler, S.P.; et al. SARS-CoV-2 infection of human ACE2-transgenic mice causes severe lung inflammation and impaired function. *Nature Immunol.* **2020**, *21*, 1327–1335. [[CrossRef](#)] [[PubMed](#)]
64. Tremblay, M.E.; Madore, C.; Bordeleau, M.; Tian, L.; Verkhratsky, A. Neuropathobiology of COVID-19: The role for glia. *Front. Cell Neurosci.* **2020**, *14*, 592214. [[CrossRef](#)]
65. Bai, L.; Zhao, Y.; Dong, J.; Liang, S.; Guo, M.; Liu, X.; Wang, X.; Huang, Z.; Sun, X.; Zhang, Z.; et al. Coinfection with influenza A virus enhances SARS-CoV-2 infectivity. *Cell Res.* **2021**, *31*, 395–403. [[CrossRef](#)]
66. Kinoshita, T.; Watanabe, K.; Sakurai, Y.; Nishi, K.; Yoshikawa, R.; Yasuda, J. Co-infection of SARS-CoV-2 and influenza virus causes more severe and prolonged pneumonia in hamsters. *Sci Rep.* **2021**, *11*, 21259. [[CrossRef](#)]
67. Askew, K.; Li, K.; Olmos-Alonso, A.; Garcia-Moreno, F.; Liang, Y.; Richardson, P.; Tipton, T.; Chapman, M.A.; Riecken, K.; Beccari, S.; et al. Coupled proliferation and apoptosis maintain the rapid turnover of microglia in the adult brain. *Cell Rep.* **2017**, *18*, 391–405. [[CrossRef](#)] [[PubMed](#)]
68. Fernández-Castañeda, A.; Lu, P.; Geraghty, A.C.; Song, E.; Lee, M.H.; Wood, J.; Yalçın, B.; Taylor, K.R.; Dutton, S.; Acosta-Alvarez, L.; et al. Mild respiratory SARS-CoV-2 infection can cause multi-lineage cellular dysregulation and myelin loss in the brain. *bioRxiv* **2022**. preprint. [[CrossRef](#)]
69. Rothan, H.A.; Kumari, P.; Stone, S.; Natekar, J.P.; Arora, K.; Auroni, T.T.; Kumar, M. SARS-CoV-2 Infects Primary Neurons from Human ACE2 Expressing Mice and Upregulates Genes Involved in the Inflammatory and Necroptotic Pathways. *Pathogens* **2022**, *11*, 257. [[CrossRef](#)]
70. Varga, Z.; Flammer, A.J.; Steiger, P.; Haberecker, M.; Andermatt, R.; Zinkernagel, A.S.; Mehra, M.R.; Schuepbach, R.A.; Ruschitzka, F.; Moch, H. Endothelial cell infection and endotheliitis in COVID-19. *Lancet* **2020**, *395*, 1417–1418. [[CrossRef](#)]
71. Colagrossi, L.; Antonello, M.; Renica, S.; Merli, M.; Matarazzo, E.; Travi, G.; Vecchi, M.; Colombo, J.; Muscatello, A.; Grasselli, G.; et al. SARS-CoV-2 RNA in plasma samples of COVID-19 affected individuals: A cross-sectional proof-of-concept study. *BMC Infect. Dis.* **2021**, *21*, 184. [[CrossRef](#)]
72. Comer, S.P.; Sullivan, S.; Szklanna, P.B.; Weiss, L.; Cullen, S.; Kelliher, S.; Smolenski, A.; Murphy, C.; Altaie, H.; Curran, J.; et al. COVID-19 induces a hyperactive phenotype in circulating platelets. *PLoS Biol.* **2021**, *19*, e3001109. [[CrossRef](#)] [[PubMed](#)]
73. Helms, J.; Tacquard, C.; Severac, F.; Leonard-Lorant, I.; Ohana, M.; Delabranche, X.; Merdji, H.; Clere-Jehl, R.; Schenck, M.; Fagot Gandet, F.; et al. High risk of thrombosis in patients with severe SARS-CoV-2 infection: A multicenter prospective cohort study. *Intensive Care Med.* **2020**, *46*, 1089–1098. [[CrossRef](#)] [[PubMed](#)]
74. Klok, F.A.; Kruip, M.J.H.A.; van der Meer, N.J.M.; Arbous, M.S.; Gommers, D.; Kant, K.M.; Kaptein, F.H.J.; van Paassen, J.; Stals, M.A.M.; Huisman, M.V.; et al. Confirmation of the high cumulative incidence of thrombotic complications in critically ill ICU patients with COVID-19: An updated analysis. *Thromb Res.* **2020**, *191*, 148–150. [[CrossRef](#)]
75. Bryche, B.; St Albin, A.; Murri, S.; Lacôte, S.; Pulido, C.; Ar Gouilh, M.; Lesellier, S.; Servat, A.; Wasniewski, M.; Picard-Meyer, E.; et al. Massive transient damage of the olfactory epithelium associated with infection of sustentacular cells by SARS-CoV-2 in golden Syrian hamsters. *Brain Behav. Immun.* **2020**, *89*, 579–586. [[CrossRef](#)] [[PubMed](#)]
76. Ye, Q.; Zhou, J.; He, Q.; Li, R.T.; Yang, G.; Zhang, Y.; Wu, S.J.; Chen, Q.; Shi, J.H.; Zhang, R.R.; et al. SARS-CoV-2 infection in the mouse olfactory system. *Cell Discov.* **2021**, *7*, 49. [[CrossRef](#)] [[PubMed](#)]
77. Dennis, A.; Wamil, M.; Kapur, S.; Alberts, J.; Badley, A.D.; Decker, G.A.; Rizza, S.A.; Banerjee, R.; Banerjee, A. Multi-organ impairment in low-risk individuals with long COVID. *medRxiv* **2020**. preprint. [[CrossRef](#)]
78. Brodin, P. Immune determinants of COVID-19 disease presentation and severity. *Nat. Med.* **2021**, *27*, 28–33. [[CrossRef](#)]
79. Baig, A.M. Deleterious outcomes in long-hauler COVID-19: The effects of SARS-CoV-2 on the CNS in chronic COVID syndrome. *ACS Chem Neurosci.* **2020**, *11*, 4017–4020. [[CrossRef](#)]
80. Doykov, I.; Hällqvist, J.; Gilmour, K.C.; Grandjean, L.; Mills, K.; Heywood, W.E. The long tail of Covid-19—The detection of a prolonged inflammatory response after a SARS-CoV-2 infection in asymptomatic and mildly affected patients. *F1000Res* **2020**, *9*, 1349. [[CrossRef](#)]

81. Arshad, U.; Pertinez, H.; Box, H.; Tatham, L.; Rajoli, R.K.R.; Curley, P.; Neary, M.; Sharp, J.; Liptrott, N.J.; Valentijn, A.; et al. Prioritization of anti-SARS-Cov-2 drug repurposing opportunities based on plasma and target site concentrations derived from their established human pharmacokinetics. *Clin. Pharmacol. Ther.* **2021**, *108*, 775–790. [CrossRef]
82. Hanafin, P.O.; Jermain, B.; Hickey, A.J.; Kabanov, A.V.; Kashuba, A.D.; Sheahan, T.P.; Rao, G.G. A mechanism-based pharmacokinetic model of remdesivir leveraging interspecies scaling to simulate COVID-19 treatment in humans. *CPT Pharmacomet. Syst. Pharmacol.* **2021**, *10*, 89–99. [CrossRef] [PubMed]
83. Rajoli, R.K.R.; Pertinez, H.; Arshad, U.; Box, H.; Tatham, L.; Curley, P.; Neary, M.; Sharp, J.; Liptrott, N.J.; Valentijn, A.; et al. Dose prediction for repurposing nitazoxanide in SARS-CoV-2 treatment or chemoprophylaxis. *Br. J. Clin. Pharmacol.* **2021**, *87*, 2078–2088. [CrossRef] [PubMed]
84. Bocan, T.M.; Basuli, F.; Stafford, R.G.; Brown, J.L.; Zhang, X.; Duplantier, A.J.; Swenson, R.E. Synthesis of [¹⁸F]Favipiravir and biodistribution in C3H/HeN Mice as assessed by positron emission tomography. *Sci. Rep.* **2019**, *9*, 1785. [CrossRef] [PubMed]
85. Painter, G.R.; Bowen, R.A.; Bluemling, G.R.; DeBergh, J.; Edpuganti, V.; Gruddanti, P.R.; Guthrie, D.B.; Hager, M.; Kuiper, D.L.; Lockwood, M.A.; et al. The prophylactic and therapeutic activity of a broadly active ribonucleoside analog in a murine model of intranasal venezuelan equine encephalitis virus infection. *Antivir. Res.* **2019**, *171*, 104597. [CrossRef]
86. EMA (European Medicines Agency). Remdesivir Gilead—Summary on Compassionate use; EMA/178637/2020; 2020. Available online: https://www.ema.europa.eu/en/documents/other/summary-compassionate-use-remdesivir-gilead_en.pdf (accessed on 8 March 2022).
87. Jorgensen, S.C.J.; Kebriaei, R.; Dresser, L.D. Remdesivir: Review of pharmacology, pre-clinical data, and emerging clinical experience for COVID-19. *Pharmacotherapy* **2020**, *40*, 659–671. [CrossRef]
88. Meijer, O.C.; de Lange, E.C.M.; Breimer, D.D.; de Boer, A.G.; Workel, J.O.; de Kloet, E.R. Penetration of dexamethasone into brain glucocorticoid targets is enhanced in mdr1A P-glycoprotein knockout mice. *Endocrinology* **1998**, *139*, 1789–1793. [CrossRef]